

Top quark physics in Vector Color-Octet Model

Sukanta Dutta^a, Ashok Goyal^{b,*} and Mukesh Kumar^{a,b†}

^a*SGTB Khalsa College, University of Delhi. Delhi-110007. India. and*

^b*Department of physics and Astrophysics, University of Delhi. Delhi-110007. India.*

We study and constrain the parameter space of the color octet vector model from the observed data at Tevatron by studying the top quark pair production and associated observables $A_{FB}^{t\bar{t}}$ and spin-correlation. In particular we study the invariant mass and rapidity dependence of $A_{FB}^{t\bar{t}}$ at Tevatron. In addition to the flavor conserving (FC) couplings we extend our study to include the flavor violating (FV) coupling involving the first and third generation quarks for both these processes. In order to ensure that we remain within the constraints imposed by the LHC data, we analyze the charge asymmetry, p_T spectrum and invariant mass in the $t\bar{t}$ production data at the LHC. The constraints from the dijet resonance searches performed by LHC are also considered. We also explore the contribution of this model to the single top quark production mediated by charged and neutral color octet vector bosons. FV couplings introduced then induce the same sign top pair production process which is analyzed for both the hadron colliders. We have incorporated the effect of finite decay width of color octets on these processes.

We find that it is possible to explain the observed $A_{FB}^{t\bar{t}}$ anomaly in the color octet vector model without transgressing the production cross-sections of all these processes both through FC and FV couplings at Tevatron. We predict best point-sets in the model parameter space for specific choices of color octet masses corresponding to χ^2_{\min} evaluated using the $m_{t\bar{t}}$ and $|\Delta y|$ spectrum of $A_{FB}^{t\bar{t}}$ from the observed data set of Run II of Tevatron at the integrated luminosity 8.7 fb^{-1} . We find that the single top quark production is more sensitive to the FC and FV couplings in comparison to the top-pair production. We provide 95 % exclusion contours on the plane of FV chiral couplings from the recent data at Tevatron, CMS and ATLAS corresponding to the non-observability of large same sign di-lepton events. The four observed point-sets are consistent with the cross section, charge asymmetry and spin-correlation measurements for $t\bar{t}$ production and dijet searches at the LHC.

Keywords: top, single-top, same-sign top, axigluons, colorons, forward-backward asymmetry, spin correlation

I. INTRODUCTION

Top quark production at high luminosity achieved at the recently shut down Tevatron has thrown tantalizing hints of physics beyond the Standard Model (SM). The combined analysis of the CDF and DØ collaboration has given results for top quark mass $m_t = 173.3 \pm 1.1 \text{ GeV}$ [1]. The current measured cross section from all channels with 4.6 fb^{-1} data is $\sigma^{t\bar{t}} = 7.5 \pm 0.31 \text{ (stat)} \pm 0.34 \text{ (syst)} \pm 0.15 \text{ (Z theory) pb}$ for $m_t = 172.5 \text{ GeV}$ [2]. For the same top mass DØ collaboration reported $\sigma^{t\bar{t}} = 7.36^{+0.90}_{-0.79} \text{ (stat+syst) pb}$ using dilepton events [3]. The leading order process for $t\bar{t}$ production at the Tevatron is $q\bar{q} \rightarrow t\bar{t}$. The top pair production cross-section with the QCD corrections at the NNLO level is computed to be $\sigma(t\bar{t})_{SM}^{NNLO} = 7.08^{+0.00+0.36}_{-0.24-0.27} \text{ pb}$ for $m_t = 173 \text{ GeV}$ [4]. These corrections are not only significant but are also in agreement with the experiment.

The CDF and DØ collaborations have reported top quark forward-backward asymmetry $A_{FB}^{t\bar{t}}$ for large $t\bar{t}$ invariant mass $m_{t\bar{t}}$ which shows a deviation of about two sigma from the SM prediction [5, 6]. Recently CDF observed the parton level $A_{FB}^{t\bar{t}}$ to be $0.296 \pm .067$ for $m_{t\bar{t}} > 450 \text{ GeV}$ based on the full Run II dataset with luminos-

ity of 8.7 fb^{-1} [7]. In the SM, this asymmetry arises only at the next to leading order through the interference between the Born term and higher order of QCD terms and is found to be 0.1 [8] which is too small to fit the data. In the literature the $A_{FB}^{t\bar{t}}$ anomaly has been attributed to new physics (NP) beyond SM [9–12]. In this article we analyze the $m_{t\bar{t}}$ and $|\Delta y|$ distributions of $A_{FB}^{t\bar{t}}$ induced by the color octet vector bosons and compare with the distribution simulated from the observed data given in reference [7]. In light of the recent observations at LHC, we constrain the new physics model parameter space from the invariant mass distribution of the $t\bar{t}$ production cross-section and the measured associated charge asymmetry.

Single top quark production is an important process at hadron colliders in providing an opportunity to probe the electroweak (EW) interactions of the top quark. Although in the SM, single top quark is produced at the EW scale, it is noteworthy that the production cross section is comparable and only a little less than half of the $t\bar{t}$ pair production. The considerable background however makes the extraction of the signal quite challenging. Recent analysis of the CDF collaboration uses 7.5 fb^{-1} of data and measures the single top quark total cross section of $\sigma_{s+t} = 3.04^{+0.57}_{-0.53} \text{ pb}$ [13]. Using 5.4 fb^{-1} of collected data, DØ at the Fermilab Tevatron Collider measured the combined single top quark production cross section $\sigma_{s+t} = 3.43^{+0.73}_{-0.74} \text{ pb}$ [14]. The predicted NNNLO approximate calculation for both the modes are $\sigma_s = 0.523^{+0.001+0.030}_{-0.005-0.028} \text{ pb}$ and $\sigma_t = 1.04^{+0.00}_{-0.02} \pm 0.06 \text{ pb}$ [4]

*Electronic address: agoyal45@yahoo.com

†Electronic address: mkumar@physics.du.ac.in

for $m_t = 173$ GeV. Recently CMS collaboration reported the t -channel EW single top quark cross section to be 83.6 ± 29.8 (stat. + syst.) ± 3.3 (lumi) pb at $\sqrt{s} = 7$ TeV at LHC [15] corresponding to integrated luminosity of 36 pb $^{-1}$, which agrees with the NLO and resummation of collinear and soft-gluon corrections NNLO [4]. However the involved experimental and theoretical uncertainties allow us to explore the new physics consequences in the determination of the production cross-section mediated by the new exotic vector bosons. Therefore it is worthwhile to study the effect of the couplings induced by the color octet vector model in the s and t channel single top quark production.

The production of same sign top quark pair is a fascinating process and would furnish unmistakable signature of physics beyond the SM. In the SM this process is highly suppressed and involves higher order flavor changing neutral current (FCNC) interactions. The search for the same sign top quark pair involves searching for events with same sign isolated leptons accompanied by hadron jets and missing transverse energy in the final state. The CDF collaboration has set a limit on same sign top pair production at Tevatron using a luminosity of 6.1 fb $^{-1}$, $\sigma(t\bar{t} + t\bar{t}) \times [\text{BR}(W \rightarrow l\nu)]^2 < 54$ fb with a 95 % confidence level [16]. This limit puts severe constraints on physics beyond the SM which allows for FCNC interactions. The 7 TeV data from CMS also disfavors the same-sign top pair production at LHC mediated through Z' in t and u channels which otherwise was the potent model to explain the $A_{FB}^{t\bar{t}}$ anomaly observed in $t\bar{t}$ production at Tevatron [17, 18]. We probe the effect of the flavor violating couplings in the same sign top pair production both at Tevatron and LHC. These couplings are introduced to contest the $A_{FB}^{t\bar{t}}$ anomaly.

In section II, we introduce the $\mathbf{3} \otimes \bar{\mathbf{3}}$ vector color octet model. In section III we compute the $t\bar{t}$ cross-section and associated top quark forward-backward asymmetry $A_{FB}^{t\bar{t}}$ and spin-correlation coefficient in this model. Single top quark production is studied in section IV and in section V we probe the same sign top quark production through FV couplings. In section VI we consider the constraints obtained by analyzing the LHC top quark data with reference to the resonance searches in $t\bar{t}$ production, dijet resonance searches and from the charge asymmetry data. Section VII is devoted to the discussion of the results and conclusion.

II. $\mathbf{3} \otimes \bar{\mathbf{3}}$ VECTOR COLOR OCTETS

The exotic bosonic states that can couple to a quark (q) and antiquark (\bar{q}) pair in physics scenarios beyond the Standard Model are the scalar/ vector color singlets, triplets, sextets and octets. Color singlet vector states are the Z 's [19], W 's [20], unparticles [9] and Kaluza-Klein gravitons G_{KK} [21]. Some of the colored exotic states are already present in some of theoretical models beyond the SM, for example R-parity violating super-symmetric

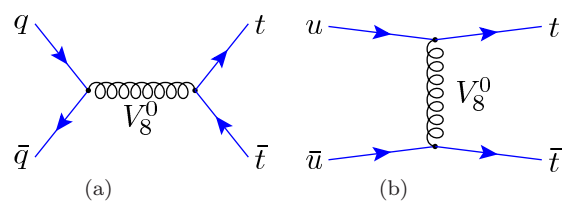


FIG. 1: Diagrams for $q\bar{q} \rightarrow t\bar{t}$ production through V_8^0 in (a) s -channel FC and (b) t -channel FV cases.

theories [22], excited quarks in composite models [23, 24], diquarks in E_6 grand unified theories [25], in theories of extra dimension [26], color-triplet and sextets [27] and in low scale string resonances [28]. Color octet scalars have been studied in reference [29] while color-octet vector states coupled to $q\bar{q}$ are analyzed in references [30, 31] for axigluons and in reference [32–34] for colorons. Some of these exotic states have been involved in the literature to explain the top quark forward-backward asymmetry and the CDF dijet resonances. These particles if they exist can be produced at LHC with their masses and couplings constrained by the measurement of the dijet cross-section at Tevatron and LHC. The ATLAS and CMS collaborations [35] have reported stringent bounds on these colored states.

In this article, we investigate the contribution of color neutral and charged vector states $V_8^{0,\mu}$ and $V_8^{\pm,\mu}$ on $t\bar{t}$ production, top-quark forward-backward asymmetry, single top quark production and same sign top pair production. The interaction of color-octet vector states $V_8^{0,\pm,\mu}$ with quark is given by

$$\begin{aligned} \mathcal{L}_{q\bar{q}V} = g_s & \left[V_8^{0a\mu} \bar{u}_i T^a \gamma_\mu (g_L^U P_L + g_R^U P_R) u_j \right. \\ & + V_8^{0a\mu} \bar{d}_i T^a \gamma_\mu (g_L^D P_L + g_R^D P_R) d_j \\ & \left. + (V_8^{+\mu} \bar{u}_i T^a \gamma_\mu (C_L P_L + C_R P_R) d_j + \text{h.c.}) \right] \end{aligned} \quad (1)$$

Since there exist stringent constraints from flavor physics on FCNC, we only consider FCNC interactions between the first and the third generation quarks only. The couplings $g_{L,R}$ and $C_{L,R}$ are free parameters in our model and taken to be diagonal. $g_s = \sqrt{4\pi\alpha_s}$ is the QCD coupling; i, j are flavor indices and a represents the color index. Production of these color-octet resonants are studied in [36] where significant bounds for these resonances based on the preliminary CMS data have been obtained. The measurement of the dijet events at Tevatron and LHC as discussed above restricts the coupling of these exotic colored states to light quark sector. The coupling of these states to top quark sector essentially remains unexplored. Here we will explore the allowed region in couplings and masses from top quark production at Tevatron and which are consistent with the LHC data and use these limits to obtain the top quark forward-backward asymmetry observed by the CDF collaboration at Tevatron [7].

We perform our calculations for top quark mass $m_t = 172.5$ GeV and bottom quark mass $m_b = 4.7$ GeV at the

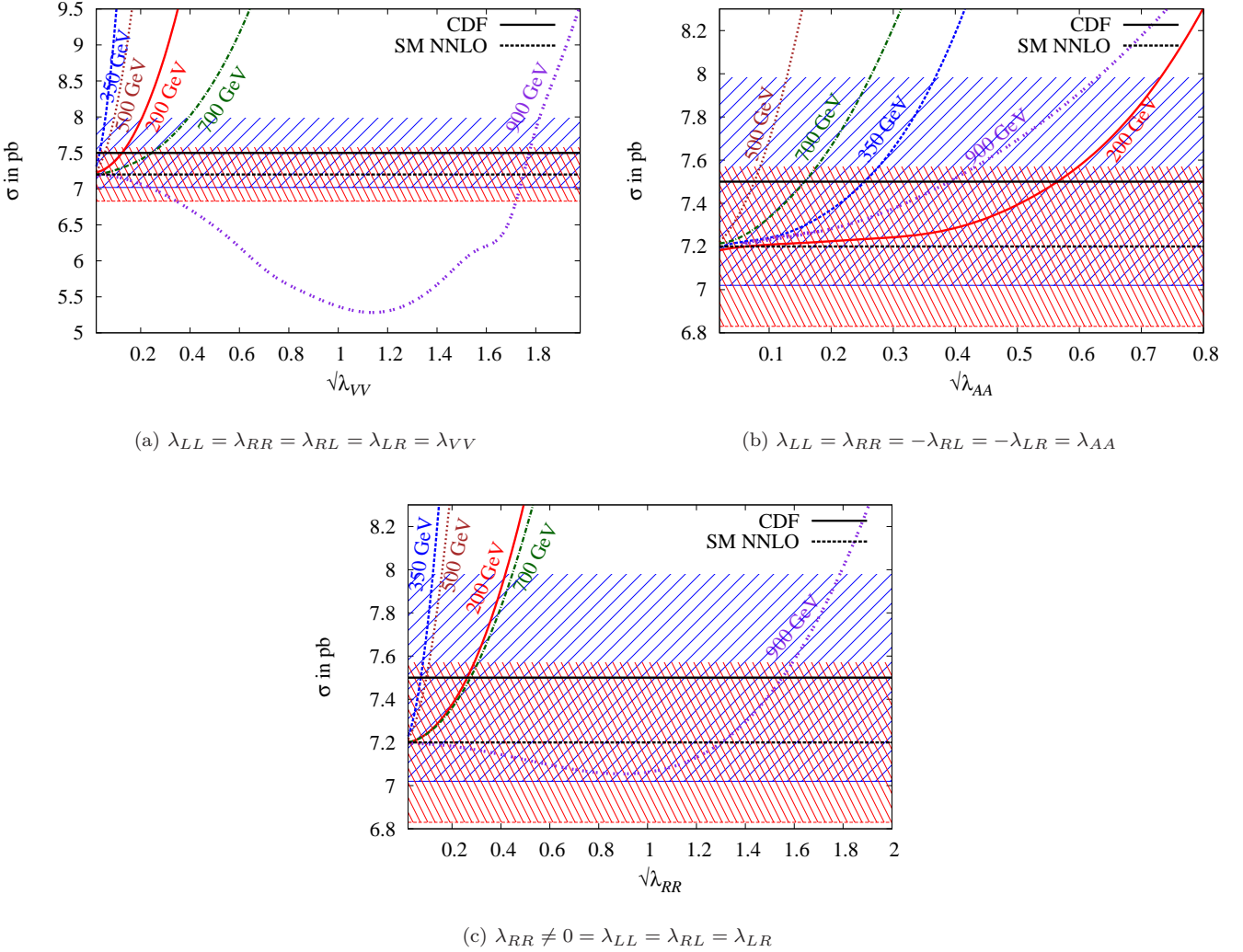


FIG. 2: Variation of the cross-section $\sigma(p\bar{p} \rightarrow t\bar{t})$ with couplings $\sqrt{\lambda}_{ij}$ for flavor conserving vector color octets corresponding to different values of $M_{V_8^0}$. The upper black dotted line associated with a blue band depicts the cross-section 7.50 ± 0.48 pb from CDF (all channels) [3], while the lower black dot-dashed line associated with a red band show theoretical estimate 7.2 ± 0.37 pb at NNLO [4]. Figures (a), (b) and (c) show the variation of σ for vector, axial and right-handed cases respectively (the cases (a), (b) and (c) as in the text).

$p\bar{p}$ center of mass energy $\sqrt{s} = 1.96$ TeV, with fixed QCD coupling $\alpha_s = 0.13$ and using CTEQ6L1 parton distribution functions keeping factorization and renormalization scales $\mu_F = \mu_R = m_t$. We have incorporated the $\mathbf{3} \otimes \mathbf{\bar{3}}$ model in MadGraph/MadEvent V4 [37] and generated a total of 10000 events for all the processes. We do not take into account the effects from parton showering, hadronization and detector conditions in our studies.

The width of the new resonances are computed and taken into consideration for all the phenomenological observables presented in this study.

III. TOP PAIR PRODUCTION

In this section we make a detailed study of $t\bar{t}$ production at the Tevatron to put bounds on the parameters of $\mathbf{3} \otimes \mathbf{\bar{3}}$ model. The new physics contribution to $t\bar{t}$ production in the present model arises through the exchange of flavor conserving and flavor violating neutral current (NC) V_8^0 as shown in figures 1a and 1b respectively. Here we assume that the flavor changing couplings are present only between the first and third generation quarks. We examine the sensitivity of both these couplings for the associated observables namely the forward-backward asymmetry and the spin correlation coefficient along with the total production cross-section.

At the Tevatron $t\bar{t}$ pair is predominantly produced

through the quark pair annihilation $q\bar{q} \rightarrow t\bar{t}$, where the quarks (anti-quarks) are mainly moving along the proton (anti-proton) direction. The FB asymmetry can be defined as

$$A_{FB} = \frac{N(\Delta y > 0) - N(\Delta y < 0)}{N(\Delta y > 0) + N(\Delta y < 0)} \quad (2)$$

where N is the number of events and $\Delta y = y_t - y_{\bar{t}}$ is the difference in rapidities of top and the anti-top quarks along the proton momentum direction in the lab frame. Recent measurements from the CDF and D0 Collaborations at the Tevatron report positive asymmetries [5] [6], $A_{FB}^{CDF} = 0.158 \pm 0.075$, $A_{FB}^{D0} = 0.196 \pm 0.065$ at the subprocess/parton level after correcting for backgrounds and detector effects corresponding to integrated luminosity of 5.3 and 5.4 fb^{-1} respectively whereas the SM prediction at NLO QCD level is 0.051 [38]. A recent report from CDF, studied FB asymmetry and its mass and rapidity dependence with an integrated luminosity of 8.7 fb^{-1} at Tevatron resulting in an inclusive parton level $A_{FB} = 0.162 \pm 0.047$ [7].

Spin-correlation of the the top-antitop pair, in the "helicity basis", (i.e; choosing the direction of the top quark momentum as our spin quantization axis) is described by four independent helicity states $\bar{t}_L t_R, \bar{t}_R t_L, \bar{t}_L t_L, \bar{t}_R t_R$. The spin-correlation parameter is defined as

$$\begin{aligned} C^{t\bar{t}} &= \frac{[\sigma(\bar{t}_R t_L) + \sigma(\bar{t}_L t_R)] - [\sigma(\bar{t}_R t_R) + \sigma(\bar{t}_L t_L)]}{[\sigma(\bar{t}_R t_L) + \sigma(\bar{t}_L t_R)] + [\sigma(\bar{t}_R t_R) + \sigma(\bar{t}_L t_L)]} \\ &= \frac{N_O - N_S}{N_O + N_S} \end{aligned} \quad (3)$$

where $N_S = \uparrow\uparrow + \downarrow\downarrow$ and $N_O = \uparrow\downarrow + \downarrow\uparrow$ are the number of top and antitop quarks with their spins parallel and anti-parallel respectively. Recent studies have shown strong spin correlation in the top quark pair production which means that the top quark and antiquark have preferential spin polarizations. At Tevatron the dominant parton level top pair production is $q\bar{q} \rightarrow t\bar{t}$ and its value for SM in the helicity basis is 0.299 [39]. CDF reported the measurement of the spin correlation coefficient $C^{t\bar{t}}_{\text{helicity}} = 0.60 \pm 0.50(\text{stat}) \pm 0.16(\text{syst})$ [40] in the helicity basis and $0.042^{+0.563}_{-0.562}$ [41] in the beam basis. Any deviation in the measurement of $C^{t\bar{t}}$ would give an indirect idea of the new $t\bar{t}$ production mechanism and also models of new physics appeal to the spin-correlation for signal identification and discrimination [43–46].

A. Flavor Conserving

The additional Feynman diagrams induced by the color octet vector bosons depicted in figure 1, interfere with the SM tree annihilation process. We take the color

octet vector boson couplings with the first two generations i.e. light quarks g_i^q ($q=u,d,s,c$) to be typically an order of magnitude smaller than the third generation heavy quarks $g_i^{t,b}$ with $i,j = L/R$. This is consistent with the dijet measurements at the Tevatron. The corresponding NP matrix element is proportional to the product of light and heavy quarks couplings. For convenience we choose the product of two couplings $\sqrt{\lambda_{ij}} = \sqrt{g_i^q g_j^t}$ and the mass $M_{V_8^0}$ as a parameter of our model in FC case. Since the total matrix element squared is left-right symmetric, we have only three independent choices of the combinations of couplings which includes the (a) vector, (b) axial-vector and (c) right-chiral interactions. All three cases can be explicitly expressed as

- (a)Vector: $g_L^q = g_R^q, g_L^t = g_R^t,$
 $\Rightarrow \lambda_{LL} = \lambda_{RR} = \lambda_{RL} = \lambda_{LR} = \lambda_{VV}$
- (b)Axial: $g_L^q = -g_R^q, g_L^t = -g_R^t,$
 $\Rightarrow \lambda_{LL} = \lambda_{RR} = -\lambda_{RL} = -\lambda_{LR} = \lambda_{AA}$
or $g_L^q = -g_R^q, g_R^t = -g_L^t$ or $g_R^q = -g_L^q, g_L^t = -g_R^t,$
 $\Rightarrow -\lambda_{LL} = -\lambda_{RR} = \lambda_{RL} = \lambda_{LR} = \lambda_{NA}$
- (c)Right-chiral: $g_L^q = g_L^t = 0,$
 $\Rightarrow \lambda_{LL} = \lambda_{LR} = \lambda_{RL} = 0 \neq \lambda_{RR}$

These massive color octets are likely to decay to the lighter quarks as well as to the heavier one if kinetically allowed both through the flavor conserving as well as flavor violating couplings. The non-zero decay width for the heavy color octets can have appreciable effects not only in the $t\bar{t}$ cross-section but also in the observables like $A_{FB}^{t\bar{t}}$ and $C^{t\bar{t}}$. The decay width of color octet vector boson is given by

$$\begin{aligned} \Gamma_{V_8} &= \frac{1}{6}\alpha_s[(g_L^2 + g_R^2)\left\{\frac{M_{V_8}^2}{2} - \frac{m_q^2 + m_{q'}^2}{4} - \left(\frac{m_q^2 - m_{q'}^2}{2M_{V_8}}\right)^2\right\} \\ &\quad + 3m_q m_{q'} g_L g_R] \frac{\lambda^{\frac{1}{2}}(M_{V_8}^2, m_q^2, m_{q'}^2)}{M_{V_8}^3} \end{aligned} \quad (4)$$

where, $\lambda(x, y, z) = x^2 + y^2 + z^2 - 2x \cdot y - 2y \cdot z - 2z \cdot x$. In flavor conserving case, for $M_{V_8} \leq 2m_t$, $q (= q') = u, d, s, c, b$ while for $M_{V_8} \geq 2m_t$ top quarks also contribute. The only flavor violating mode we have is $V_8^0 \rightarrow u\bar{t} + \bar{u}t$. The decay of the charged color octet vector boson $V_8^\pm \rightarrow qq'$ proceeds through the exotic charge current (CC) interactions which are assumed to diagonal but with non-universal coupling to the third generation quark sector.

Throughout our analysis we have taken into account the effect of the finite decaywidth in evaluating the cross-sections and other associated observables.

The analytical expression of differential cross-section in terms of λ_{ij} for $q\bar{q} \rightarrow t\bar{t}$ with respect to the cosine of the top quark polar angle θ in the $t\bar{t}$ center-of-mass (c.m.) frame is given as

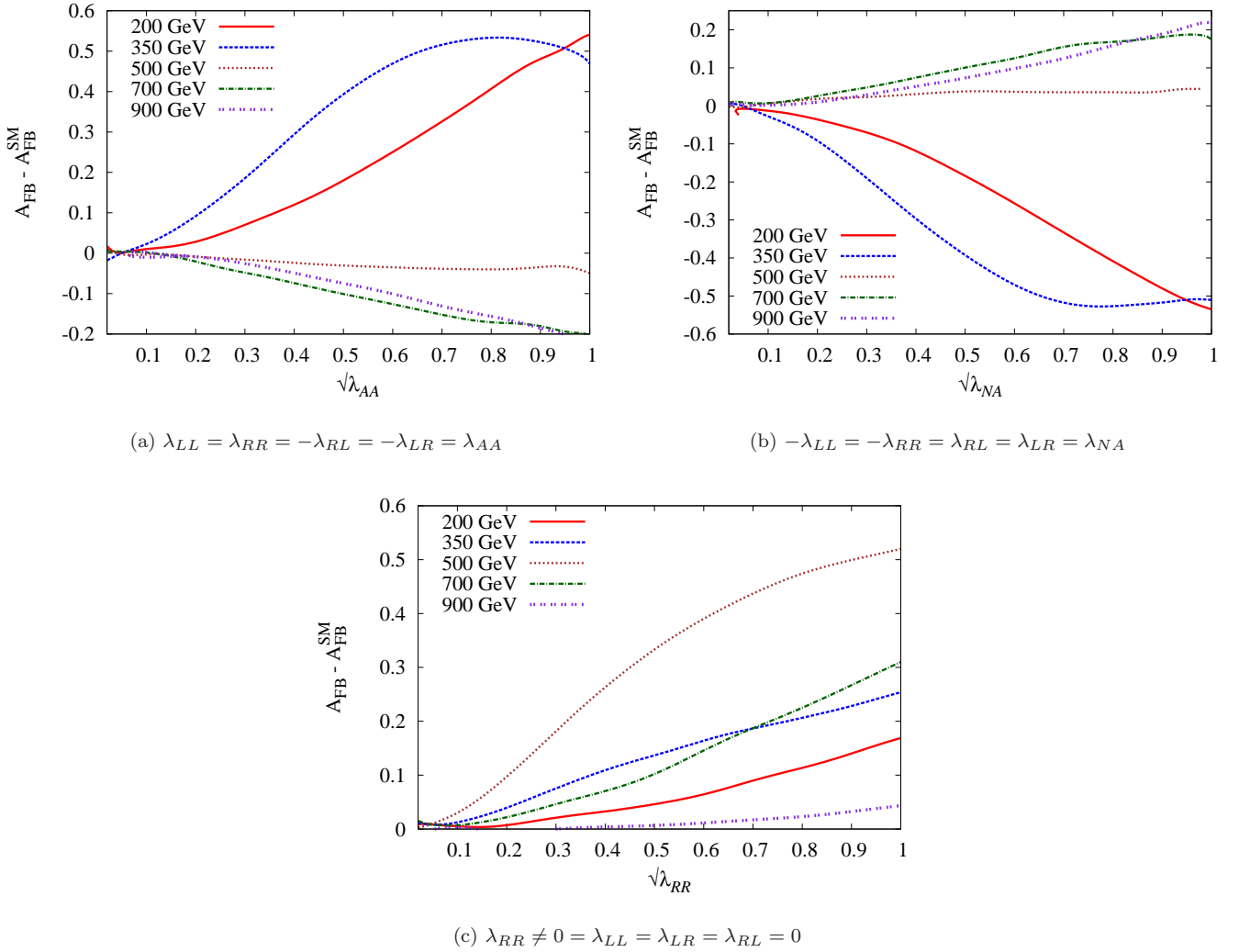


FIG. 3: Variation of the $A_{FB} - A_{FB}^{SM}$ with couplings $\sqrt{\lambda}_{ij}$ for flavor conserving vector color octets corresponding to different values of $M_{V_8^0}$. Figures (a), (b) and (c) corresponds to the positive product of axial couplings, negative product of axial couplings and purely right-handed cases (the first two corresponds to cases (b) and the third corresponds to case (c) in the text respectively). The $A_{FB}^{t\bar{t}}$ for case (a) vanishes identically for all mass regions.

$$\frac{d\hat{\sigma}}{d \cos\theta} = \frac{\pi\beta\alpha_s^2}{9\hat{s}} \left[f(\theta, \beta^2) + \left\{ \left(1 - \frac{M_{V_8^0}^2}{\hat{s}} \right)^2 + \frac{M_{V_8^0}^2}{\hat{s}} \frac{\Gamma_{V_8^0}^2}{\hat{s}} \right\}^{-1} \left\{ (\lambda_{LR}^2 + \lambda_{RL}^2 + \lambda_{LL}^2 + \lambda_{RR}^2)(2 - \sin^2\theta) \frac{\beta^2}{4} \right. \right. \\ + ((\lambda_{LL} + \lambda_{LR})^2 + (\lambda_{RL} + \lambda_{RR})^2) \frac{1 - \beta^2}{4} + \frac{1}{2} \left(1 - \frac{M_{V_8^0}^2}{\hat{s}} \right) (\lambda_{LL} + \lambda_{RR} + \lambda_{LR} + \lambda_{RL}) f(\theta, \beta^2) \\ \left. \left. + \left(\left(1 - \frac{M_{V_8^0}^2}{\hat{s}} \right) (\lambda_{LL} + \lambda_{RR} - \lambda_{LR} - \lambda_{RL}) + \frac{1}{4} (\lambda_{LL}^2 + \lambda_{RR}^2 - \lambda_{LR}^2 - \lambda_{RL}^2) \right) \beta \cos\theta \right\} \right] \quad (5)$$

where $\hat{s} = (p_q + p_{\bar{q}})^2$ is the squared c.m. energy of the system, $\beta = \sqrt{1 - 4m_t^2/\hat{s}}$ is the top quark velocity and $f(\theta, \beta^2) = (2 - \beta^2 \sin^2\theta)$. The terms proportional to

$\cos\theta$ in equation (5) are sensitive to the forward backward asymmetry. In figures 2, 3 and 4 we plot the variation of the cross section, the forward backward asym-

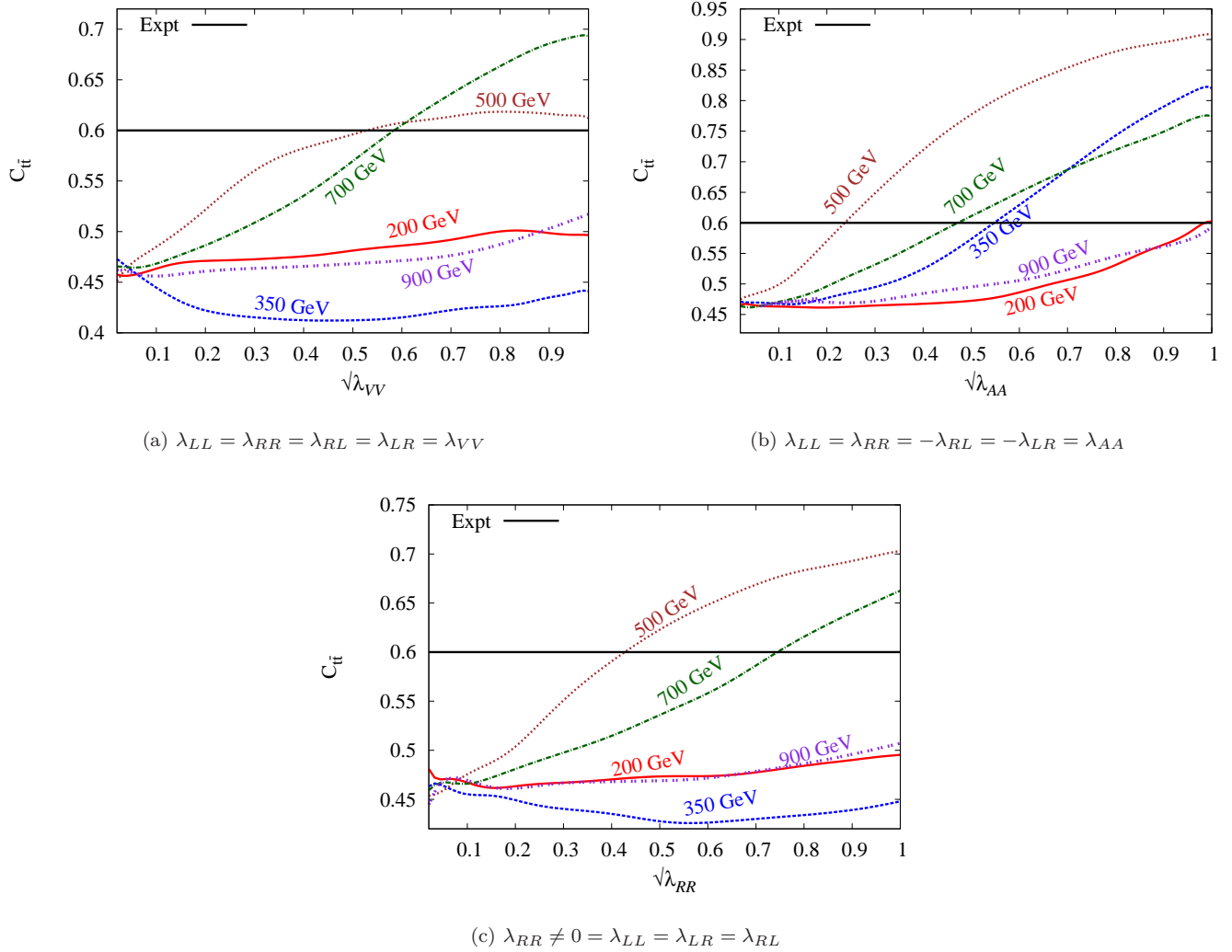


FIG. 4: Variation of the spin-correlation coefficient $C^{t\bar{t}}$ with couplings $\sqrt{\lambda_{ij}}$ for flavor conserving vector color octets corresponding to different values of $M_{V_8^0}$. Figures (a), (b) and (c) correspond to vector, axial and right-handed cases respectively (cases (a), (b) and (d) in the text respectively). The spin-correlation variation for cases (c) and (b) as in text are identical.

metry $A_{FB}^{t\bar{t}}$ and the spin correlation $C_{t\bar{t}}$ respectively as a function of coupling $\sqrt{\lambda_{ij}}$.

We look at three different regions based on the octet masses and the threshold of top-pair production, region I where $M_{V_8^0} \ll 2m_t$, region II $M_{V_8^0} - \Gamma_{V_8^0} \leq 2m_t \leq M_{V_8^0} + \Gamma_{V_8^0}$ and region III where $M_{V_8^0} \gg 2m_t$ respectively. Figures 2a corresponds to the case (a), which implies pure vector interactions. For $M_{V_8^0} = 200$ GeV which lies in region I, the cross-section grows with coupling due to the positive interference inspite of the s channel suppression. For $M_{V_8^0} = 350$ - 500 GeV which lies in the resonant region II, we have a much sharper rise in the cross-section with the increasing coupling. For higher octet masses we observe the effect of negative interference with SM as long as the coupling $|\lambda_{ij}| \leq 1$ and then it gradually grows with the couplings due to the dominance of the new physics squared term. However, pure vector interactions fail to

generate the $A_{FB}^{t\bar{t}}$.

Figure 2b corresponds to phenomenologically interesting case (b), which is purely an axial interaction and thus generates a large forward-backward asymmetry. Since the interference terms contributing to the cross-section vanish in this case and only the squared term grows with coupling, we observe that this generates an increasing $A_{FB}^{t\bar{t}}$ without enhancing the cross-section for the couplings $|\lambda_{ij}| \leq 1$. However for the higher masses in region III, the $A_{FB}^{t\bar{t}}$ becomes negative due to the negative interference with SM as shown in figure 3b.

The fair amount of $A_{FB}^{t\bar{t}}$ can also be generated through axial current for large masses by taking the negative product of the axial couplings of light quark and top quark, keeping the cross-section same as before. We depict the $A_{FB}^{t\bar{t}}$ contribution for the negative product of axial couplings in figure 3a.

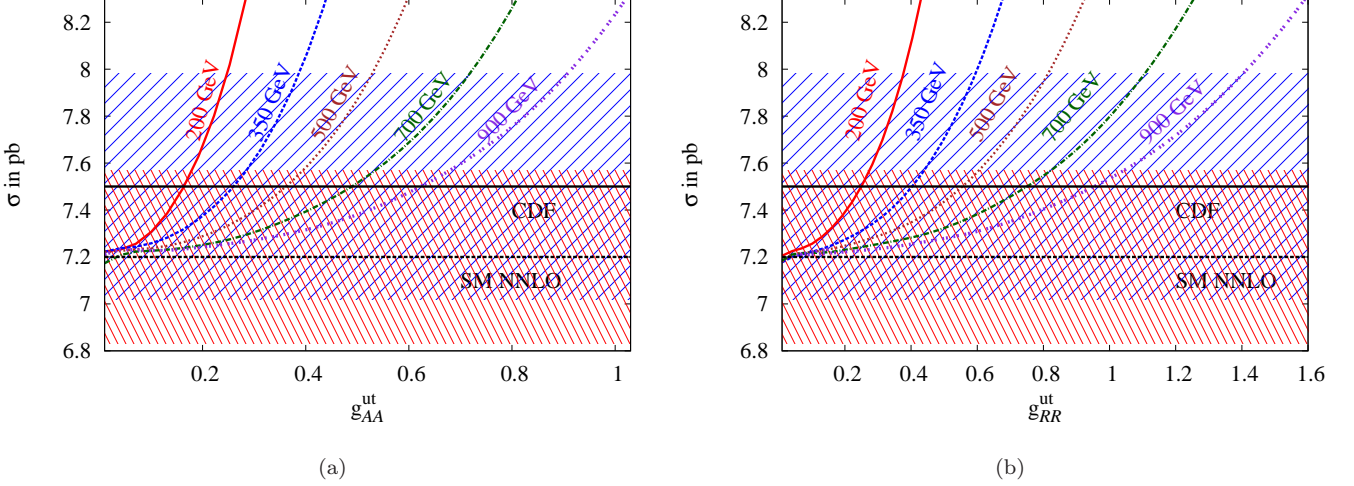


FIG. 5: Variation of the cross-section $\sigma(p\bar{p} \rightarrow t\bar{t})$ with couplings g_{ij}^{ut} for flavor violating vector color octets corresponding to different values of $M_{V_8^0}$. The upper black dotted line associated with a blue band depicts the cross-section 7.50 ± 0.48 pb from CDF (all channels) [3], while the lower black dot-dashed line associated with a red band show theoretical estimate 7.2 ± 0.37 pb at NNLO [4]. Figures (a) and (b) show the variation of σ for axial vector and right-handed cases (the cases (a) and (b) of the text respectively).

Variation of cross-section for case (c) is given in figure 2c which is similar to case (a). In this case we get positive A_{FB} for all the cases but it grows faster for $M_{V_8^0} = 500$ GeV with respect to $\sqrt{\lambda_{RR}}$ comparing to other two masses of V_8^0 as shown in figure 3c.

The behavior of the variation of the spin correlation

coefficients can be understood by exhibiting the total matrix element squared as a combination of the same and opposite helicity amplitudes. The differential cross section corresponding to the same and opposite helicity amplitudes are

$$\frac{d\hat{\sigma}_S^{\text{FC}}}{d\cos\theta} = g_s^4(1-\beta^2)\sin^2\theta \left[8 + \frac{2\hat{s}(\hat{s}-M_{V_8^0}^2)}{(\hat{s}-m_{V_8^0}^2)^2 + \Gamma_{V_8^0}^2 M_{V_8^0}^2} (\lambda_{LL} + \lambda_{RR} + \lambda_{LR} + \lambda_{RL}) \right. \\ \left. + \frac{\hat{s}^2}{(\hat{s}-M_{V_8^0}^2)^2 + \Gamma_{V_8^0}^2 M_{V_8^0}^2} (\lambda_{LL}^2 + \lambda_{RR}^2 + \lambda_{LR}^2 + \lambda_{RL}^2 + 2(\lambda_{LL}\lambda_{LR} + \lambda_{RL}\lambda_{RR})) \right] \quad (6)$$

$$\frac{d\hat{\sigma}_O^{\text{FC}}}{d\cos\theta} = g_s^4(1+\cos^2\theta) \left[8 + \frac{\hat{s}(\hat{s}-M_{V_8^0}^2)}{(\hat{s}-M_{V_8^0}^2)^2 + \Gamma_{V_8^0}^2 M_{V_8^0}^2} (\lambda_{LL} + \lambda_{RR} + \lambda_{LR} + \lambda_{RL}) \right. \\ \left. + \frac{\hat{s}^2}{(\hat{s}-M_{V_8^0}^2)^2 + \Gamma_{V_8^0}^2 M_{V_8^0}^2} \left\{ (1+\beta^2)(\lambda_{LL}^2 + \lambda_{RR}^2 + \lambda_{LR}^2 + \lambda_{RL}^2) + 2(1-\beta^2)(\lambda_{LL}\lambda_{LR} + \lambda_{RL}\lambda_{RR}) \right\} \right] \\ + g_s^4(2\beta\cos\theta) \left[\frac{\hat{s}(\hat{s}-M_{V_8^0}^2)}{(\hat{s}-M_{V_8^0}^2)^2 + \Gamma_{V_8^0}^2 M_{V_8^0}^2} (\lambda_{LL} + \lambda_{RR} - \lambda_{LR} - \lambda_{RL}) \right. \\ \left. + \frac{\hat{s}^2}{(\hat{s}-M_{V_8^0}^2)^2 + \Gamma_{V_8^0}^2 M_{V_8^0}^2} 2(\lambda_{LL}^2 + \lambda_{RR}^2 - \lambda_{LR}^2 - \lambda_{RL}^2) \right] \quad (7)$$

Examining equations (6) and (7), we find that for case (a), the contribution from the $\frac{d\hat{\sigma}_S^{\text{FC}}}{d\cos\theta}$ is suppressed by the

factor $(1-\beta^2)\sin^2\theta / (1+\cos^2\theta)$ w.r.t. $\frac{d\hat{\sigma}_O^{\text{FC}}}{d\cos\theta}$, while for the case (b), only new physics squared term from $\frac{d\hat{\sigma}_O^{\text{FC}}}{d\cos\theta}$

contributes to the spin correlation coefficient. For the right chiral current case (c), we observe that for the interference term the ratio is again suppressed by the same factor as in case (a), while it is further suppressed by the factor $1/(1+\beta^2)$ for the squared term. Therefore it is evident that $C^{t\bar{t}}$ is likely to increase with the increasing coupling products.

Variation of spin correlation coefficient $C^{t\bar{t}}$ with respect to $\sqrt{\lambda_{ij}}$ has almost similar behavior for all the cases considered as shown in figures 4a -4c. Here the $C^{t\bar{t}}$ in region I first decreases with couplings due to negative interference and then increases due to the dominance of the squared term. For the octet mass 350 GeV at the region II the $C^{t\bar{t}}$ registers the minimum value showing that at threshold production it is likely to have an equal number of parallel and antiparallel states. In axial case (b) and (c), since there is no interference, the $C^{t\bar{t}}$ increases with couplings for all mass regions which is evident from figure 4b.

B. Flavor Violating

In the flavor violating case, apart from the usual SM diagrams we have t -channel diagrams for $u\bar{u} \rightarrow t\bar{t}$ with V_8^0 as shown in figure 1b which interfere with the corresponding s -channel SM diagrams initiated with u and \bar{u} partons. The flavor violating neutral coupling is considered only among the first and third generation u and t quarks g_i^{ut} ($i = L, R$) with V_8^0 . In contrast to the flavor conserving case, here we consider only two choices of coupling combinations (a) $g_L^{ut} = g_R^{ut}$ or $g_L^{ut} = -g_R^{ut}$ and (b) $g_L^{ut} = 0$ or $g_R^{ut} = 0$ to study the three observables because corresponding matrix element square is symmetric in both the cases. The differential cross-section in terms of flavor violating neutral coupling g_i^{ut} for $u\bar{u} \rightarrow t\bar{t}$ with QCD s -channel and additional t -channel diagram through V_8^0 (NP) with respect to the cosine of the top quark polar angle θ in the $t\bar{t}$ center-of-mass (c.m.) frame is

$$\frac{d\hat{\sigma}}{d \cos \theta} = \frac{\pi \beta \alpha_s^2}{9\hat{s}} \left(2 - \beta^2 \sin^2 \theta \right) - \frac{\pi \beta \alpha_s^2}{54\hat{s}^2} \frac{\hat{s}^2(\hat{t} - M_{V_8^0}^2)}{(\hat{t} - M_{V_8^0}^2)^2 + \Gamma_{V_8^0}^2 M_{V_8^0}^2} (1 + \beta \cos \theta)^2 (g_L^{ut2} + g_R^{ut2}) \\ + \frac{\pi \beta \alpha_s^2}{36\hat{s}} \frac{\hat{s}^2}{(\hat{t} - M_{V_8^0}^2)^2 + \Gamma_{V_8^0}^2 M_{V_8^0}^2} \left[(g_L^{ut4} + g_R^{ut4}) (1 + \beta \cos \theta)^2 + 8g_L^{ut2} g_R^{ut2} (1 + \beta^2) \right] \quad (8)$$

where $\hat{t} = (p_u - p_t)^2 = (p_{\bar{u}} - p_{\bar{t}})^2$.

Figure 5 shows the variation of cross-section as a function of coupling g_{ij}^{ut} , ($i, j = L$ or R) for both cases (a) and (b) for different $M_{V_8^0}$ same as in FC case.

We observe the growth of the cross-section with the couplings due to the overall positive interference in equation (8) generated from large negative value of \hat{t} . It is also observed that the variations are comparatively flat w.r.t. the corresponding cases of the flavor conserving scenarios due to the suppressed \hat{t} channel propagator $(\hat{t} - m_{V_8^0}^2)^2 + \Gamma_{V_8^0}^2 M_{V_8^0}^2$ in the interference term.

A_{FB} as a function of couplings for both cases is plotted in figure 6. We find that A_{FB} is positive in both cases and increases with coupling, the increase being more rapid for lower mass.

The behavior of $C^{t\bar{t}}$ can be studied by writing the matrix element squared in terms of the same and opposite helicity contributions as before. From equations (A.3)-(A.5), we define $\frac{d\hat{\sigma}_S^{FV}}{d \cos \theta}$ and $\frac{d\hat{\sigma}_O^{FV}}{d \cos \theta}$ as

$$\frac{d\hat{\sigma}_S^{FV}}{d \cos \theta} = g_s^4 (1 - \beta^2) \sin^2 \theta \left[8 + \frac{2}{3} \frac{\hat{s}(\hat{t} - M_{V_8^0}^2)}{(\hat{t} - M_{V_8^0}^2)^2 + \Gamma_{V_8^0}^2 M_{V_8^0}^2} (g_L^{ut2} + g_R^{ut2}) + \frac{\hat{s}^2}{(\hat{t} - M_{V_8^0}^2)^2 + \Gamma_{V_8^0}^2 M_{V_8^0}^2} (g_L^{ut4} + g_R^{ut4}) \right] \\ + 8 g_s^4 \frac{\hat{s}^2}{(\hat{t} - M_{V_8^0}^2)^2 + \Gamma_{V_8^0}^2 M_{V_8^0}^2} g_L^{ut2} g_R^{ut2} (1 + \beta^2) \quad (9)$$

$$\frac{d\hat{\sigma}_O^{FV}}{d \cos \theta} = g_s^4 (1 + \cos^2 \theta) \left[8 + \frac{2}{3} \frac{\hat{s}(\hat{t} - M_{V_8^0}^2)}{(\hat{t} - M_{V_8^0}^2)^2 + \Gamma_{V_8^0}^2 M_{V_8^0}^2} (g_L^{ut2} + g_R^{ut2}) + \frac{\hat{s}^2}{(\hat{t} - M_{V_8^0}^2)^2 + \Gamma_{V_8^0}^2 M_{V_8^0}^2} (g_L^{ut4} + g_R^{ut4})(1 + \beta^2) \right] \\ + g_s^4 (2\beta \cos \theta) \left[\frac{2}{3} \frac{\hat{s}(\hat{t} - M_{V_8^0}^2)}{(\hat{t} - M_{V_8^0}^2)^2 + \Gamma_{V_8^0}^2 M_{V_8^0}^2} (g_L^{ut2} + g_R^{ut2}) + \frac{2\hat{s}^2}{(\hat{t} - M_{V_8^0}^2)^2 + \Gamma_{V_8^0}^2 M_{V_8^0}^2} (g_L^{ut4} + g_R^{ut4}) \right] \quad (10)$$

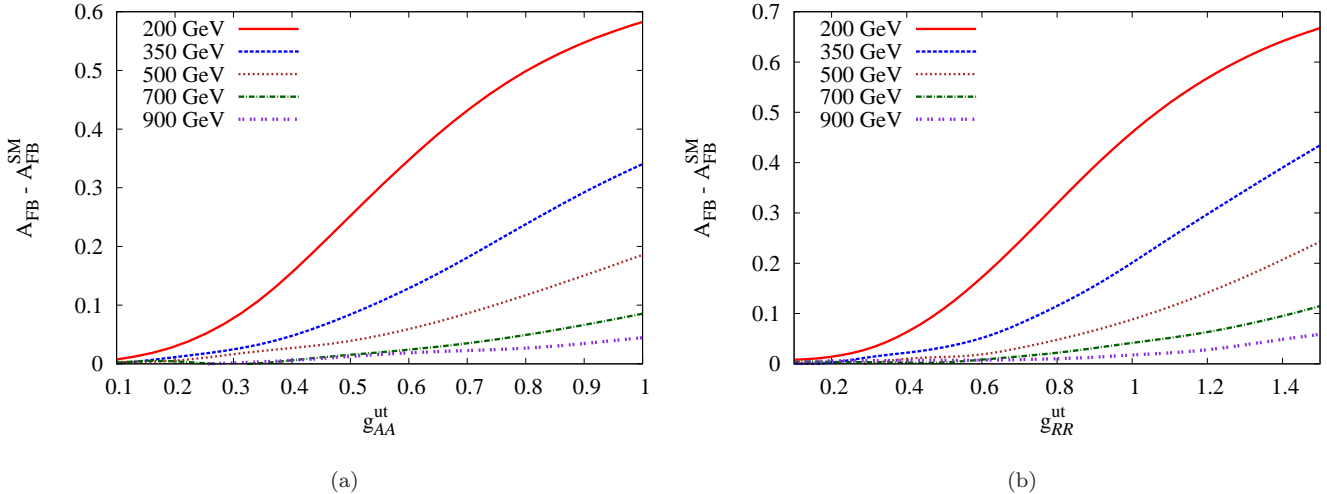


FIG. 6: Variation of the $A_{FB} - A_{FB}^{SM}$ with couplings g_{ijt}^u for flavor violating vector color octets corresponding to different values of M_{V^0} . Figures (a) and (b) corresponds to axial vector and right-handed cases (the cases (a) and (b) of the text respectively).

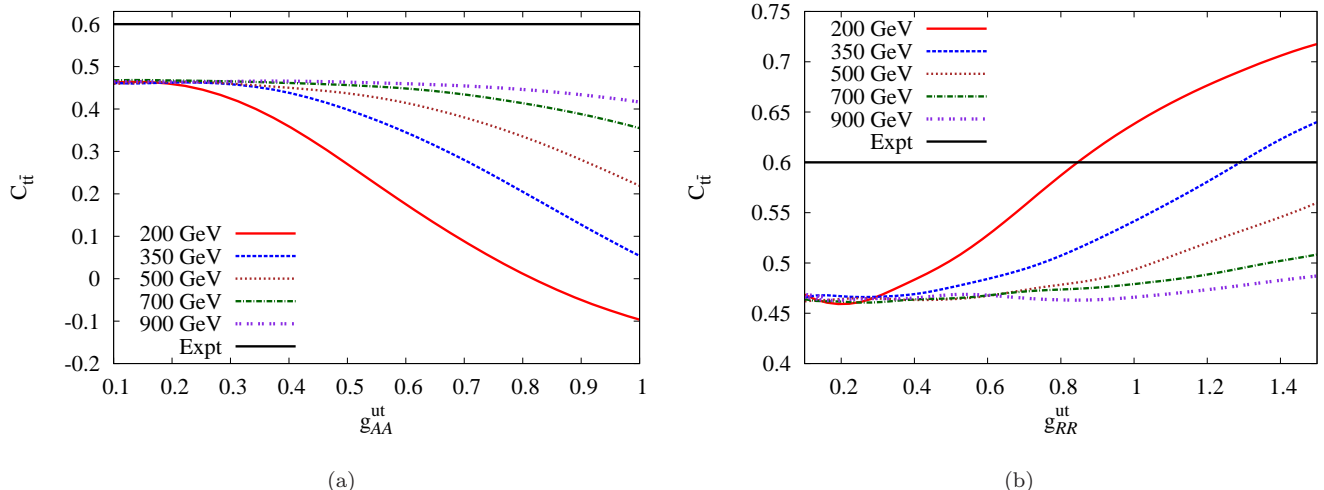


FIG. 7: Variation of the spin-correlation coefficient C^{tt} with couplings g_{ij}^{ut} for flavor violating vector color octets corresponding to different values of $M_{V_8^0}$. Figures (a) and (b) corresponds to axial vector and right-handed cases (the cases (a) and (b) of the text respectively).

Analyzing the expression given in equations (9) and (10) we find that the contribution of $\frac{d\hat{\sigma}_S^{FV}}{d \cos \theta}$ in vector/axial-vector case dominates over the $\frac{d\hat{\sigma}_O^{FV}}{d \cos \theta}$ due to the presence of the cross term proportional to $(g_L^{ut} g_R^{ut})^2$ and hence spin-correlation decreases with the coupling as shown in the figure figure 7a. In contrast, this cross term vanishes for the pure right handed interactions and then the $\frac{d\hat{\sigma}_S^{FV}}{d \cos \theta}$ is suppressed by $(1 - \beta^2) \sin^2 \theta / (1 + \beta^2)(1 + \cos^2 \theta)$ w.r.t. $\frac{d\hat{\sigma}_O^{FV}}{d \cos \theta}$, rendering C^{tt} to increase with the coupling as shown in figure 7b.

Our results are in broad agreement with the existing results in the literature [30–33]. Their study was however based on the earlier results from Tevatron [5] with the $A_{FB}^{t\bar{t}}$ dependence on $m_{t\bar{t}}$ in two regions of ≤ 450 GeV and ≥ 450 GeV respectively.

C. χ^2 Analysis

We have studied the production cross-section and also the model contribution to the observables. We further analyze the one dimensional distribution plots

and investigate the possibility to explain the observed $A_{FB}^{t\bar{t}}$ anomaly. Recently CDF collaboration have performed detail seven bin analysis with invariant mass distribution of $A_{FB}^{t\bar{t}}$ from the reconstructed top-pairs [7]. They observed that the large forward-backward asymmetry comes from the higher invariant mass $M_{t\bar{t}}$ bins of the top-antitop pair. The forward-backward asymmetry as a function of $M_{t\bar{t}}$ is defined as

$$A_{FB}(M_{t\bar{t}}) = \frac{N_F(M_{t\bar{t}}) - N_B(M_{t\bar{t}})}{N_F(M_{t\bar{t}}) + N_B(M_{t\bar{t}})} \quad (11)$$

where N_F and N_B are the events in the forward and backward region respectively. The analysis in reference [7] also gives the four bin analysis of the $A_{FB}^{t\bar{t}}$ with the top-antitop rapidity difference distribution defined as

$$A_{FB}(|\Delta y|) = \frac{N(\Delta y > 0) - N(\Delta y < 0)}{N(\Delta y > 0) + N(\Delta y < 0)} \quad (12)$$

where rapidity difference $\Delta y = y_t - y_{\bar{t}}$, $N(\Delta y < 0)$ and $N(\Delta y > 0)$ are the number of events with positive and negative rapidity difference respectively.

We scan our model parameter space for a given mass of the color octet vector boson on the two dimensional plane of two distinct product of couplings which can provide the matched $m_{t\bar{t}}$ and Δy distribution of $A_{FB}^{t\bar{t}}$ with the observed data. We perform χ^2 analysis for both FC and FV cases and predict the set of best parameters which can possibly explain the $A_{FB}^{t\bar{t}}$ anomaly. To make this χ^2 study we take into account the $A_{FB}^{t\bar{t}}$ distribution over $m_{t\bar{t}}$ bins as well as Δy bins from the full Run II Tevatron Dataset [7]. We define the combined χ^2 from the study of the $m_{t\bar{t}}$ and Δy distribution as For these

analysis we use standard χ^2 fit, defined as

$$\chi^2 = \sum_i \frac{(\mathcal{O}_i^{\text{th}} - \mathcal{O}_i^{\text{exp}})^2}{(\delta \mathcal{O}_i)^2} \quad (13)$$

where i is the $m_{t\bar{t}}$ or Δy bin index, $\mathcal{O}_i^{\text{th}}$ and $\mathcal{O}_i^{\text{exp}}$ are model and experimental estimate of the $A_{FB}^{t\bar{t}}$ in the i^{th} bin respectively. The model estimate includes the both SM and new physics contribution. $\delta \mathcal{O}_i$ is the the experimental error in the corresponding i^{th} bin. We have considered seven and four suggested bins for the $m_{t\bar{t}}$ and Δy respectively. In addition we have also considered the total cross-section $\sigma(pp \rightarrow t\bar{t}) = 7.5 \pm 0.31(\text{stat}) \pm 0.34(\text{syst}) \pm 0.15(\text{Z theory}) \text{ pb}$ [2] as one of the observed data. Therefore we have used twelve observables to perform the analysis. For $\mathcal{O}_i^{\text{th}}$ we have taken the total cross-section for this study as $\sigma^{\text{tot}} = K \cdot \sigma^{\text{SM}} + \sigma^{\text{NP}}$, where $K = \frac{\sigma^{\text{NLO}}}{\sigma^{\text{SM}}} = 1.046$ and $A_{FB}^{t\bar{t}} = A_{FB}^{t\bar{t} \text{ SM NLO}} + A_{FB}^{t\bar{t} \text{ NP}}$.

The two dimensional parameter space ($(\sqrt{\lambda_{LL}}, \sqrt{\lambda_{RR}})$ for FC cases and $(g_L^{\text{ut}}, g_R^{\text{ut}})$ for the FV case) with a given fixed mass is scanned leading to the minimum value of the $\chi^2 \equiv \chi_{\min}^2$. We plot histograms showing the $m_{t\bar{t}}$ spectrum of $A_{FB}^{t\bar{t}}$ at combined χ_{\min}^2 in figures 8a, 8e, 8c for flavor conserving cases and 9a, 9c and 9e for flavor violating cases respectively. We have shown and compared the slope of our best-fit line with that from the experimental data in these figures and tables I and III. Similarly figures 8b, 8f, 8d for flavor conserving cases and 9b, 9d and 9f for flavor violating cases exhibit the Δy spectrum of $A_{FB}^{t\bar{t}}$ at combined χ_{\min}^2 along with the slope of the best fit line. These values for the Δy distribution of $A_{FB}^{t\bar{t}}$ are also summarized in tables II and IV.

$M_{t\bar{t}}$	$A_{FB}^{t\bar{t}} (\pm \text{ stat.})$	NLO $t\bar{t}$ -Bkg	200 GeV $\sqrt{\lambda_{AA}} = 0.30$	900 GeV $\sqrt{\lambda_{NAA}} = 0.35$	500 GeV $\sqrt{\lambda_{RR}} = 0.11$
< 400 GeV	-0.012 \pm 0.040	0.012	0.055	0.024	0.018
400 – 450 GeV	0.084 \pm 0.050	0.031	0.101	0.074	0.005
450 – 500 GeV	0.158 \pm 0.064	0.039	0.172	0.062	0.105
500 – 550 GeV	0.203 \pm 0.083	0.060	0.135	0.118	0.254
550 – 600 GeV	0.143 \pm 0.105	0.083	0.208	0.145	0.113
600 – 700 GeV	0.338 \pm 0.128	0.077	0.172	0.230	0.142
≥ 700 GeV	0.377 \pm 0.163	0.137	0.329	0.282	0.230
χ_{\min}^2	-	-	6.05	5.27	7.43
Slope of Best-Fit Line	$(11.1 \pm 2.9) \times 10^{-4}$	3.0×10^{-4}	6.08×10^{-4}	7.04×10^{-4}	5.31×10^{-4}

TABLE I: The first three columns give the bin limits of the $M_{t\bar{t}}$, the observed $A_{FB}^{t\bar{t}}$ with error and the NLO (QCD+EW) generated $A_{FB}^{t\bar{t}}$ respectively [7]. The next three consecutive columns provide the differential $A_{FB}^{t\bar{t}}$ corresponding to the model parameters (given in figures 8a, 8e, and 8c) leading to χ_{\min}^2 at fixed coupling and $M_{V_8^0}$ in flavor conserving cases. The penultimate line gives the χ_{\min}^2 for respective cases. The last line in the table gives the slope of the best fit line with the simulated data.

IV. SINGLE TOP

In the SM, single top quark production is studied through three different channels with different final states

respectively which have their own distinct kinematics and

$ \Delta y $	$A_{FB}^{t\bar{t}}$ (\pm stat.)	NLO $t\bar{t}$ -Bkg	200 GeV $\sqrt{\lambda_{AA}} = 0.30$	900 GeV $\sqrt{\lambda_{NAA}} = 0.35$	500 GeV $\sqrt{\lambda_{RR}} = 0.11$
0.0-0.5	0.026 ± 0.035	0.009	0.046	0.018	0.015
0.5-1.0	0.065 ± 0.045	0.040	0.142	0.068	0.089
1.0-1.5	0.269 ± 0.066	0.074	0.209	0.184	0.133
≥ 1.5	0.299 ± 0.126	0.113	0.223	0.249	0.266
χ^2_{\min}	-	-	4.41	1.87	4.73
Slope of Best-Fit Line	$(20.0 \pm 5.9) \times 10^{-2}$	6.7×10^{-2}	11.96×10^{-2}	16.18×10^{-2}	15.94×10^{-2}

TABLE II: The first three columns give the bin limits of the $|\Delta y|$, the observed $A_{FB}^{t\bar{t}}$ with error and the NLO (QCD+EW) generated $A_{FB}^{t\bar{t}}$ respectively [7]. The next three consecutive columns provide the differential $A_{FB}^{t\bar{t}}$ corresponding to the model parameters (given in figures 8b, 8f and 8d) leading to χ^2_{\min} at fixed coupling and $M_{V_8^0}$ in flavor conserving cases. The penultimate line gives the χ^2_{\min} for respective cases. The last line in the table gives the slope of the best fit line with the simulated data.

$M_{t\bar{t}}$	200 GeV	500 GeV	900 GeV
	$g_{AA}^{ut} = 0.26$	$g_{AA}^{ut} = 0.53$	$g_{RR}^{ut} = 1.26$
< 400 GeV	0.037	0.019	0.023
400 – 450 GeV	0.031	0.053	0.073
450 – 500 GeV	0.095	0.110	0.089
500 – 550 GeV	0.188	0.160	0.121
550 – 600 GeV	0.134	0.194	0.163
600 – 700 GeV	0.256	0.207	0.182
≥ 700 GeV	0.263	0.267	0.297
χ^2_{\min}	4.92	4.14	4.93
Slope of Best-fit Line	6.85×10^{-4}	6.6×10^{-4}	6.74×10^{-4}

TABLE III: Same as TABLE I, first column give the bin limits of the $M_{t\bar{t}}$ and the next three consecutive columns provide the differential $A_{FB}^{t\bar{t}}$ corresponding to the model parameters (given in figures 9a, 9c and 9e leading to χ^2_{\min} in flavor violating cases.

do not interfere with one another. The s -channel process takes place through an off-shell time like W boson which further decay into a top and bottom quark as shown in figure 10a. The t -channel process is the dominant one and mediates through the exchange of a virtual W as shown in figure 10c. The t -channel process resembles deep inelastic scattering while s -channel process resembles the Drell-Yan process. The single top quark production cross-section in these two modes have been estimated to be $\sigma_{t\text{-channel}}^{NNNLO} = 1.05 \pm 0.11$ pb, $\sigma_{s\text{-channel}}^{NNNLO} = 0.52 \pm 0.03$ pb respectively at the NNNLO approximation for $m_t = 173$ GeV [4]. Therefore the single top quark production in the t -channel is roughly twice of the s -channel production cross-section in the SM. The third channel for single top production is the associated tW -production as shown in figure 10b which is estimated to be $\sigma_{Wt\text{-channel}}^{NNNLO} = 0.11 \pm 0.04$ pb for $m_t = 173$ GeV [4]. We do not consider this process for our analysis. The single top quark production cross-section in the t -channel is thus expected to dominate over the s -channel production both at the Tevatron and LHC while the cross-section for tW production is very small at Tevatron but significant at the LHC. The three channels discussed above are sensitive to quite different manifestations of physics beyond the SM such that Flavor Changing Neutral Current (FCNC), existence of color singlet / octet vector bosons $W'^\pm, H^\pm, Z', V_8^{\pm,0}$ etc, fourth gen-

eration quarks or detection of more general four fermion interactions. DØ reported the s - and t - channel cross-sections to be $\sigma_s = 0.68_{-0.35}^{+0.38}$ pb and $\sigma_t = 2.86_{-0.63}^{+0.69}$ pb for $m_t = 172.5$ GeV respectively [14] in agreement with the estimated cross-sections in the SM. However, very recently CDF collaboration [13] using 7.5 fb^{-1} of $p\bar{p}$ collisions data collected by CDF Run II experiment channel as $\sigma_s = 1.81_{-0.58}^{+0.63}$ pb and $\sigma_t = 1.49_{-0.42}^{+0.47}$ pb where in the central values of s - and t -channel cross-sections are comparable which is in conflict with the SM NNNLO prediction. The total single top cross-section measured by this group $\sigma_{total} = 3.04_{-0.53}^{+0.57}$ pb for $m_t = 172.5$ GeV is however consistent with the total single top production in SM at the NNNLO approximation.

There are two alternative approaches available in the literature to study t - channel single top quark production at the leading order (LO) and next to leading order (NLO). One of the approach is based on $2 \rightarrow 2$ scattering process figure 10c, where b quark is taken to be present in the initial state. This is so called five flavor (5F) scheme. In this scheme the presence of b jet and the effect of b mass appears only at NLO. In the second approach the LO (Born process) is the $2 \rightarrow 3$ scattering process figure 10d. In this four flavor (4F) scheme, the b quark does not enter in the QCD evaluation of the PDF's. For details see [47] [48]. The approaches are shown to be equivalent and give the same result at all orders in the

$ \Delta y $	200 GeV $g_{AA}^{ut} = 0.26$	500 GeV $g_{AA}^{ut} = 0.53$	900 GeV $g_{RR}^{ut} = 1.26$
0.0-0.5	0.031	0.022	0.035
0.5-1.0	0.072	0.101	0.077
1.0-1.5	0.139	0.149	0.149
≥ 1.5	0.317	0.260	0.235
$\chi^2_{\min.}$	3.97	4.03	3.71
Slope of Best-fit Line	18.5×10^{-2}	15.24×10^{-2}	13.44×10^{-2}

TABLE IV: Same as TABLE II, first column give the bin limits of the $|\Delta y|$ and the next three consecutive columns provide the differential $A_{FB}^{t\bar{t}}$ corresponding to the model parameters (given in figures 9b, 9d and 9f leading to $\chi^2_{\min.}$ in flavor violating cases.

perturbation expansion. In the present work we treat proton in 5F scheme and study the b -initiated $2 \rightarrow 2$ process since we are only interested in estimation of the total production cross-section [49].

In this section we will study single top s - and t -channel production in $\mathbf{3} \otimes \bar{\mathbf{3}}$ model in flavor conserving and flavor violating cases. Throughout our analysis we assume $|V_{tb}| = 1$. In the flavor conserving case, the single top production in the s - and t -channels proceeds through the charge current interactions through V_8^\pm as shown in figures 11a and 11b respectively. The flavor violating mode mediates through flavor changing neutral current via V_8^0 as shown in figures 11c and 11d respectively. The charged octet vector boson do not contribute to the

other processes in the top quark sector addressed in our study. However, the contribution of the FCNC is likely to provide the common global allowed parameter space of the model from all the processes involving the top quark sector.

A. Flavor Conserving

The differential cross-sections with respect to emerging angle of the single massive top quark $\cos \theta_t$ the s -channel subprocess $u\bar{d} \rightarrow t\bar{b}$, and the t -channel subprocess $u\bar{b} \rightarrow t\bar{d}$ are given as

$$\frac{d\sigma_{u\bar{d} \rightarrow t\bar{b}}}{d \cos \theta_t} = \frac{\pi \beta' \alpha_s^2}{18\hat{s}} \frac{1}{(\hat{s} - M_{V_8}^2)^2 + M_{V_8}^2 \Gamma_{V_8}^2} \left[\mathcal{C}_+ \hat{u}(\hat{u} - m_t^2) + \mathcal{C}_- \hat{t}(\hat{t} - m_t^2) \right], \quad (14)$$

$$\frac{d\sigma_{u\bar{b} \rightarrow t\bar{d}}}{d \cos \theta_t} = \frac{\pi \beta' \alpha_s^2}{18\hat{s}} \frac{1}{(\hat{t} - M_{V_8}^2)^2 + M_{V_8}^2 \Gamma_{V_8}^2} \left[\mathcal{C}_+ \hat{s}(\hat{s} - m_t^2) + \mathcal{C}_- \hat{t}(\hat{t} - m_t^2) \right], \quad (15)$$

$$\text{where } \mathcal{C}_\pm = (|C_L^{tb}|^2 + |C_R^{tb}|^2)(|C_L^{ud}|^2 + |C_R^{ud}|^2) \pm (|C_L^{tb}|^2 - |C_R^{tb}|^2)(|C_L^{ud}|^2 - |C_R^{ud}|^2) \quad \text{and } \beta' = 1 - \frac{m_t^2}{\hat{s}} \quad (16)$$

It is evident from the equation (16) that the contribution for the pure vector current and pure axial current is identical which also hold true between the right and left chiral contributions. We study the variation of the single top quark production in the s channel with the couplings for various vector octet masses which are shown in figures 12a and 12b corresponding to the charged axial and right chiral current respectively. We observe the sharp growth in the cross-sections even with the smaller couplings and later flattens out with the increasing mass of the octet.

Figures 12c and 12d depicts the variation in the t channel mode. It is evident that the plugging of decay width in t channel propagator flattens the variation of the curve *w.r.t.* couplings. Since there is no interference between the SM and color octet model (for both the channels), we find that the cross-section grows with the coupling and decreases with the mass of the color octet vector bosons.

B. Flavor Violating

FCNC induces additional channels for single top quark production. These additional Feynman diagrams are shown in figures 11c and 11d. This contribution is realized through the flavor changing coupling $g_{L,R}^{ut}$ at one of the vertices only but can be mediated through both s and t channels. This then would make the life uncomfortable for measuring s and t channel separately as the final states for both the diagrams are same. In this view for this we need to have a combined study of s and t channel with one FV vertex from the new physics sector. Thus the new physics contribution at the amplitude level is proportional to the product of the flavor conserving cou-

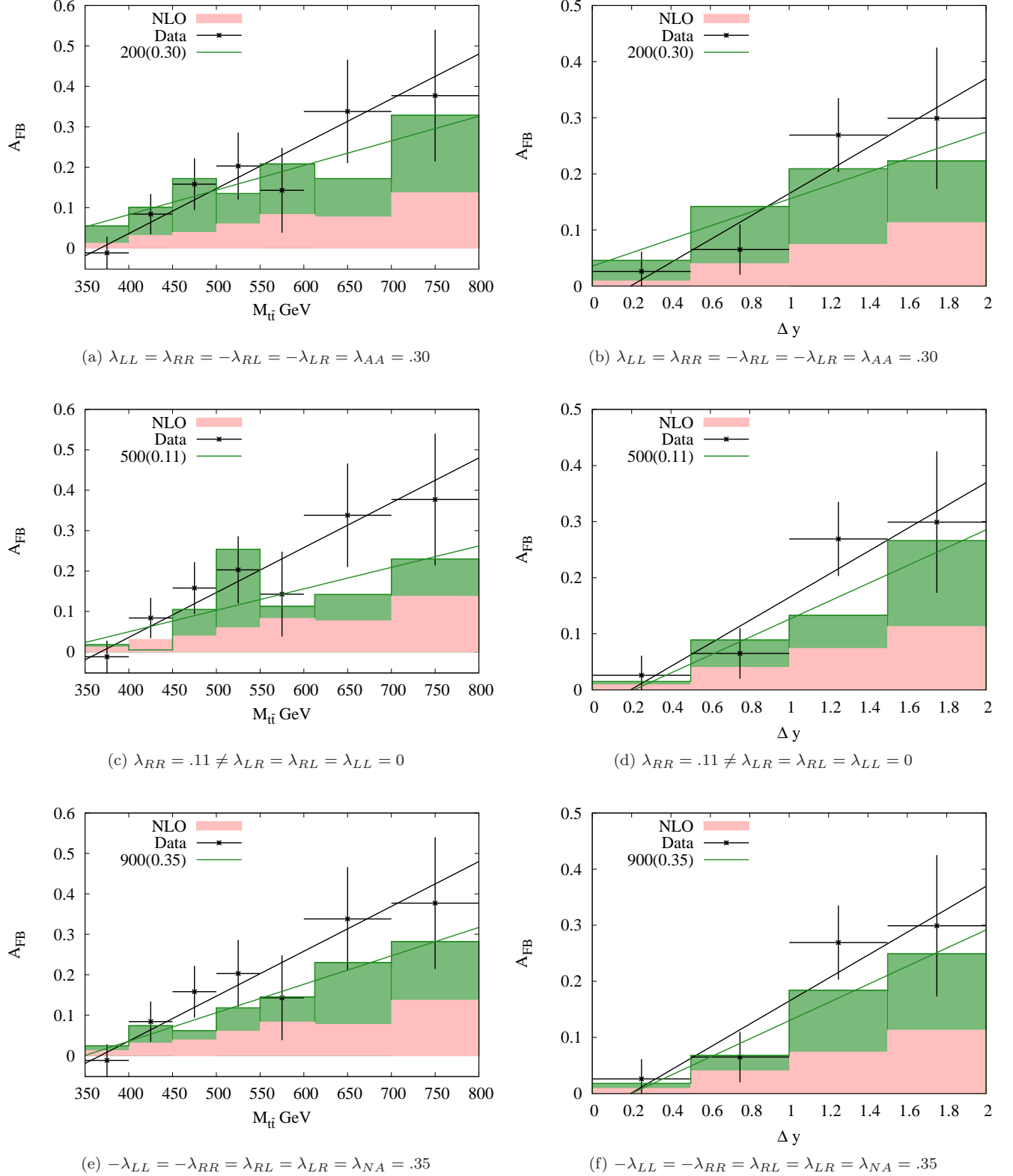


FIG. 8: $m_{t\bar{t}}$ and $|\Delta y|$ distribution of $A_{FB}^{t\bar{t}}$ at χ^2_{\min} , for the three favorable point-sets in parameter space at fixed $M_{V_8^0} = 200, 500$ and 900 GeV for flavor conserving case, shown in the shaded green histogram. The experimental data point is shown with its error in black, while the SM (NLO+QCD) with background subtracted are shown in the shaded pink histogram. The black line in all graphs is the best-fit line with the experimental data while the green line depicts the best-fit line with the model data.

pling $g_{L,R}^q$ and flavor violating coupling $g_{L,R}^{ut}$. We define $\sqrt{f_{ij}^{q,ut}} = \sqrt{g_i^q g_j^{ut}}$ for $i \equiv L, R, V, A$. The differential cross-section with respect to $\cos\theta_t$ for the s -channel sub-

process $q\bar{q} \rightarrow t\bar{u}(q = d, s, c, b)$, $s + t$ -channel subprocess $u\bar{u} \rightarrow t\bar{u}$ and $t + u$ -channel subprocess $uu \rightarrow tu$ assuming top quark mass m_t and others to be massless is given as

$$\frac{d\sigma_{q\bar{q} \rightarrow t\bar{u}}}{d\cos\theta_t} = \frac{\pi\beta'\alpha_s^2}{18\hat{s}} \frac{1}{(\hat{s} - M_{V_8^0}^2)^2 + M_{V_8^0}^2\Gamma_{V_8^0}^2} \left[\mathcal{V}_+ \hat{u}(\hat{u} - m_t^2) + \mathcal{V}_- \hat{t}(\hat{t} - m_t^2) \right] \quad (17)$$

$$\begin{aligned} \frac{d\sigma_{u\bar{u} \rightarrow t\bar{u}}}{d\cos\theta_t} = & \frac{\pi\beta'\alpha_s^2}{18\hat{s}} \left\{ \frac{1}{(\hat{s} - M_{V_8^0}^2)^2 + M_{V_8^0}^2\Gamma_{V_8^0}^2} \left[\mathcal{V}_+ \hat{u}(\hat{u} - m_t^2) + \mathcal{V}_- \hat{t}(\hat{t} - m_t^2) \right] \right. \\ & - \frac{2}{3} \frac{(\hat{s} - M_{V_8^0}^2)}{(\hat{s} - M_{V_8^0}^2)^2 + M_{V_8^0}^2\Gamma_{V_8^0}^2} \frac{(\hat{t} - M_{V_8^0}^2)}{(\hat{t} - M_{V_8^0}^2)^2 + M_{V_8^0}^2\Gamma_{V_8^0}^2} \hat{u}(\hat{u} - m_t^2) \left[(g_L^{uu} g_L^{ut})^2 + g_R^{uu} g_R^{ut})^2 \right] \\ & \left. + \frac{1}{(\hat{t} - M_{V_8^0}^2)^2 + M_{V_8^0}^2\Gamma_{V_8^0}^2} \left[\mathcal{V}_+ \hat{s}(\hat{s} - m_t^2) + \mathcal{V}_- \hat{u}(\hat{u} - m_t^2) \right] \right\} \end{aligned} \quad (18)$$

$$\begin{aligned} \frac{d\sigma_{uu \rightarrow tu}}{d\cos\theta_t} = & \frac{\pi\beta'\alpha_s^2}{18\hat{s}} \left\{ \frac{1}{(\hat{t} - M_{V_8^0}^2)^2 + M_{V_8^0}^2\Gamma_{V_8^0}^2} \left[\mathcal{V}_+ \hat{u}(\hat{u} - m_t^2) + \mathcal{V}_- \hat{s}(\hat{s} - m_t^2) \right] \right. \\ & + \frac{2(\hat{t} - M_{V_8^0}^2)(\hat{u} - M_{V_8^0}^2)}{((\hat{t} - M_{V_8^0}^2)^2 + M_{V_8^0}^2\Gamma_{V_8^0}^2)((\hat{u} - M_{V_8^0}^2)^2 + M_{V_8^0}^2\Gamma_{V_8^0}^2)} \hat{s}(\hat{s} - m_t^2) \left[(g_L^{uu} g_L^{ut})^2 + g_R^{uu} g_R^{ut})^2 \right] \\ & \left. + \frac{1}{(\hat{u} - M_{V_8^0}^2)^2 + M_{V_8^0}^2\Gamma_{V_8^0}^2} \left[\mathcal{V}_+ \hat{t}(\hat{t} - m_t^2) + \mathcal{V}_- \hat{s}(\hat{s} - m_t^2) \right] \right\} \end{aligned} \quad (19)$$

where $\mathcal{V}_{\pm} = (|g_L^{ut}|^2 + |g_R^{ut}|^2)(|g_L^{qq}|^2 + |g_R^{qq}|^2) \pm (|g_L^{ut}|^2 - |g_R^{ut}|^2)(|g_L^{qq}|^2 - |g_R^{qq}|^2)$

Since the amplitude is the quadratic symmetric function of the left and right handed couplings, the axial and vector currents are identical and so is the case for right and left handed currents. We have also taken into account of the additional decay channels contributing to the total decay width of the color octet neutral vector boson due to the introduction of FV couplings. We exhibit the variation of the single top quark production with the product of the couplings $\sqrt{f_{ij}^{q,ut}}$ for different flavor violating color octet neutral vector boson masses in figure 13a and 13b corresponding to the axial and right chiral current. We observe the the coupling f_i are quite sensitive to the production cross-section for the cases. It would then imply that for a given FC coupling the single top production can constrain the FV coupling more severely than the top-pair production.

V. SAME-SIGN TOP

Introduction of the flavor violating couplings involving first and third generation for the top-pair production

also induces the new channel for same sign top/ anti-top pair production. The same sign top production is highly suppressed in SM because it involves higher order flavor changing neutral current interactions.

In the present study the process $uu(\bar{u}\bar{u}) \rightarrow tt(\bar{t}\bar{t})$ proceeds through the exchange of neutral color octet vector boson V_8^0 with flavor changing neutral current interactions between the first and third generation only in the t -channel and the exchange diagram u -channel as shown in figure 14.

The differential cross-section for $uu(\bar{u}\bar{u}) \rightarrow tt(\bar{t}\bar{t})$ with respect to the cosine of the top quark polar angle θ in the tt center-of-mass (c.m.) frame is

$$\frac{d\hat{\sigma}}{d\cos\theta} = \frac{\pi\beta'\alpha_s^2}{(\hat{t} - M_{V_8^0}^2)^2 + M_{V_8^0}^2\Gamma_{V_8^0}^2} \frac{\hat{s}}{18} \left[2(g_L^{ut4} + g_R^{ut4}) + g_L^{ut2} g_R^{ut2} (1 + \beta\cos\theta)^2 \right]$$

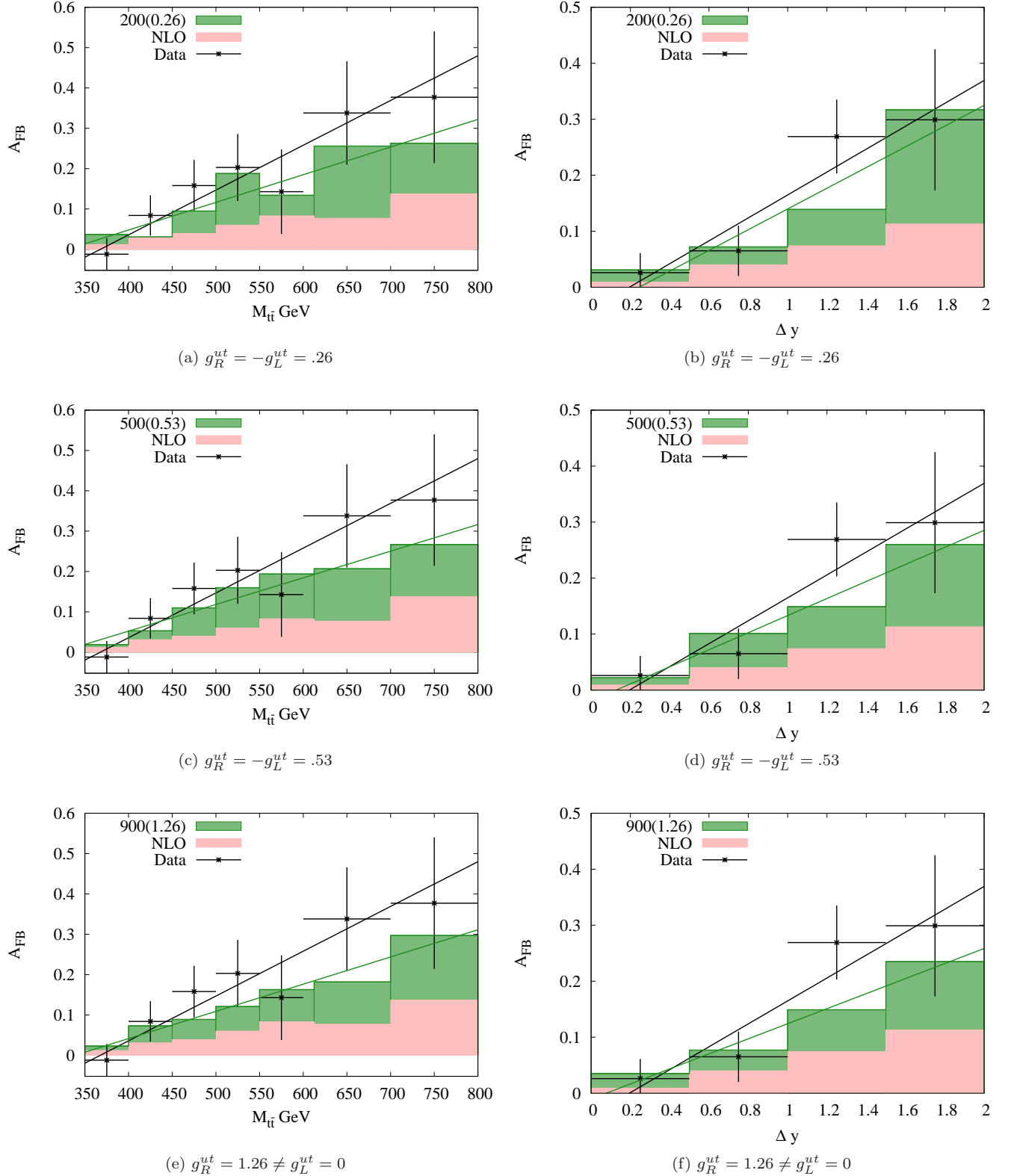
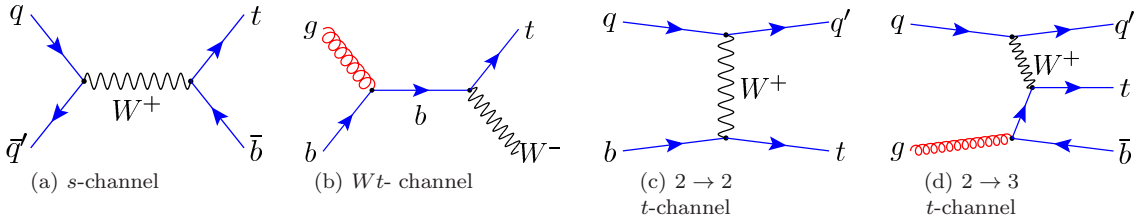
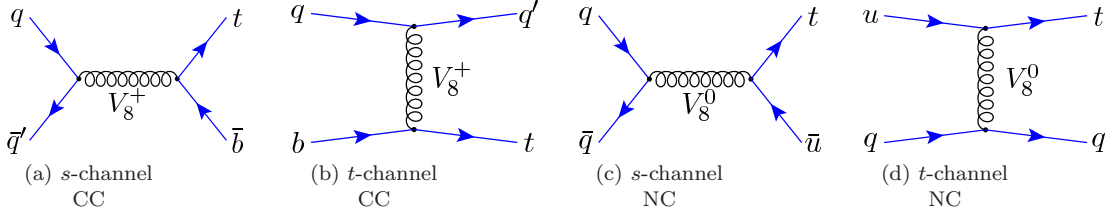


FIG. 9: $m_{t\bar{t}}$ and $|\Delta y|$ distribution of $A_{FB}^{t\bar{t}}$ at χ^2_{\min} , for the three favorable point-sets in parameter space at fixed $M_{V_8^0} = 200, 500$ and 900 GeV for flavor violating case, shown in the shaded green histogram. The experimental data point is shown with its error in black, while the SM (NLO+QCD) with background subtracted are shown in the shaded pink histogram. The black line in all graphs is the best-fit line with the experimental data while the green line depicts the best-fit line with the model data.

FIG. 10: *Leading order single top production channels in SM.*FIG. 11: *Leading order single top production channels mediated by charged color octet vector current are shown in figures (a)-(b) and flavor violating neutral color octet vector current are shown in figures (d)-(e) respectively.*

$$\begin{aligned}
& + \frac{2\pi\beta\alpha_s^2(\hat{t} - m_{V_8^0}^2)(\hat{u} - m_{V_8^0}^2)}{((\hat{t} - M_{V_8^0}^2)^2 + M_{V_8^0}^2\Gamma_{V_8^0}^2)((\hat{u} - M_{V_8^0}^2)^2 + M_{V_8^0}^2\Gamma_{V_8^0}^2)} \frac{\hat{s}}{9} \left[(g_L^{ut4} + g_R^{ut4}) - 2g_L^{ut2}g_R^{ut2}\frac{m_t^2}{\hat{s}} \right] \\
& + \frac{\pi\beta\alpha_s^2}{(\hat{u} - M_{V_8^0}^2)^2 + M_{V_8^0}^2\Gamma_{V_8^0}^2} \frac{\hat{s}}{18} \left[2(g_L^{ut4} + g_R^{ut4}) + g_L^{ut2}g_R^{ut2}(1 - \beta\cos\theta)^2 \right]
\end{aligned} \quad (20)$$

where $\hat{s} = (p_u + p_{\bar{u}})^2$ is the squared c.m. energy of the system with top quark velocity $\beta = \sqrt{1 - 4m_t^2/\hat{s}}$.

We study the variation of the production cross-section $\sigma(p\bar{p} \rightarrow tt + \bar{t}t)$ w.r.t. axial vector and right chiral FCNC couplings respectively. To compare with the experimental results we allow these tops/ antitops to decay through leptonic channels only as shown in figures 15a and 15b. However, the non observability of same sign dilepton events at the hadronic colliders restricts the parameter space of the model generating such events. In figure 16a we depict the constrain on the left and right chiral couplings from the observed cross-section of $\sigma(p\bar{p} \rightarrow tt + \bar{t}t) \times BR[W \rightarrow l\nu]^2 \leq 0.54$ pb for the combined signature of the same sign top pair and same sign anti-top pair production and then decaying through the respective leptonic channels [16]. CMS [17] and ATLAS [18] data constrains the parameter space from $\sigma(pp \rightarrow tt)$ only with observed cross-section ≤ 17 pb and ≤ 1.7 pb respectively. Figures 16b and 16c provides the 95 % confidence level exclusion contours in the two dimensional plane of flavor violating chiral couplings g_L^{ut} and g_R^{ut} for a given color octet mass corresponding to the observed data from CMS and ATLAS respectively.

We observe that these contours severely narrows the allowed parameter space contributing to the top-antitop pair production and generating the positive A_{FB}^{tt} .

VI. CONSISTENCY WITH THE $t\bar{t}$ AND DIJET PRODUCTION AT LHC

In the previous section we investigated the parameter region for color octet vector bosons and found constraints on the masses and couplings by taking total top quark pair production at Tevatron including single top quark production and same-sign top quark production cross sections. We then analyzed the exclusion region of the parameters via same-sign top quark pair production at Tevatron as well as at the LHC. Additionally, fitted data for A_{FB}^{tt} at the Tevatron restricted the parameter space further and gave some favorable parameters in the model considered in this article. Further investigations can then lead to exclusion/acceptance of the parameters by studying transverse momentum of the final states and invariant mass differential distributions for top pair and dijet production cross sections. The other observables like S, T parameters and the Z decay width effects further constraint the color octet vector boson model but these studies are beyond the scope of this article, detail studies can be found in [50]. In this section we investigate the consistency of the favorable parameters found at Tevatron by studying the cross section, charge asymmetry, spin-correlation, invariant mass differential distributions for top quark pair production and dijets production data at the LHC.

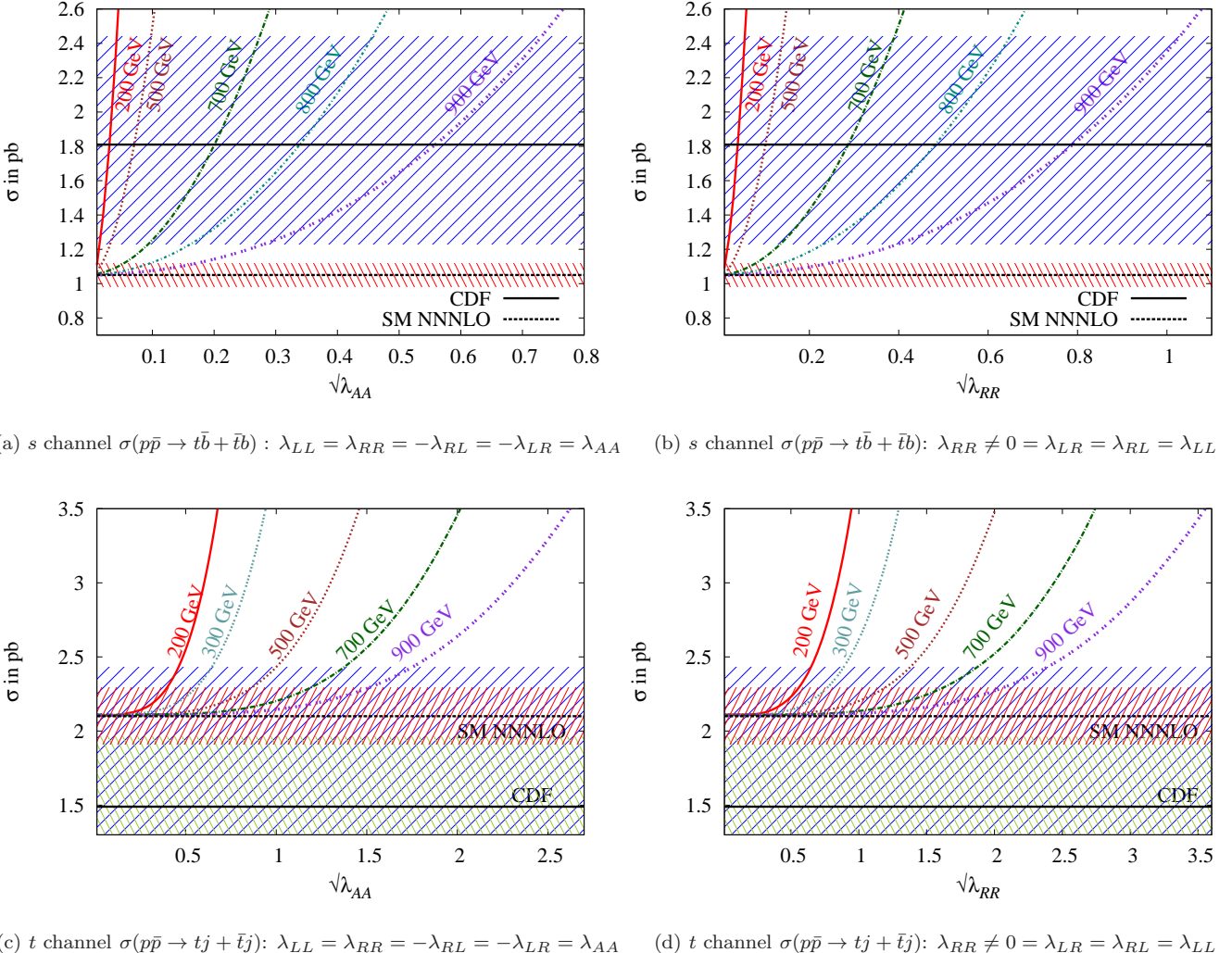
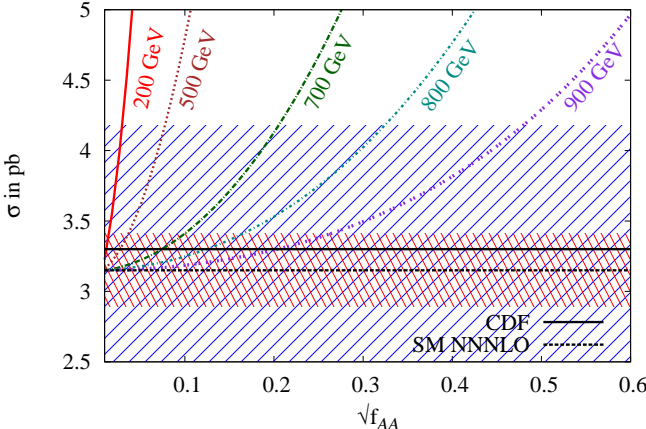


FIG. 12: Variation of the cross-section with flavor conserving couplings for various vector color octet masses $M_{V_8^\pm}$. In the top panel figures (a) and (b) the upper dotted black line and associated blue band depicts the CDF central value and the one sigma band respectively for s -channel cross-section $1.81^{+0.63}_{-0.58}$ pb [13], while the lower dot-dashed black line with a red band show theoretical central value and the one sigma band respectively for 1.05 ± 0.07 pb at NNNLO [4]. Similarly in the lower panel figures (c) and (d) the experimental central value is shown with lower dotted black line and the associated 1-sigma green band, 2-sigma blue band corresponds to t -channel cross-section $1.49^{+0.47}_{-0.42}$ pb from CDF [13]. The upper dot-dashed black line associated with a red band show theoretical central value and one sigma band for 2.10 ± 0.19 pb at NNNLO [4].

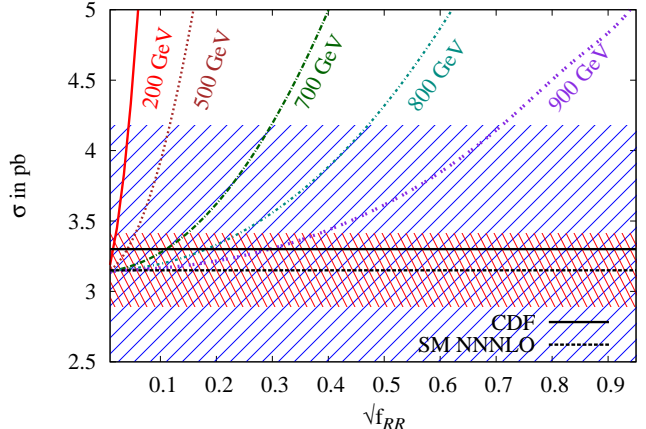
A. $t\bar{t}$ production and $m_{t\bar{t}}$ distribution

The color octet vector bosons not only contribute to the $t\bar{t}$ production cross section both at the Tevatron and the LHC but modify its shape as a function of invariant mass $m_{t\bar{t}}$ as well. The $t\bar{t}$ resonance searches will put constraints on the resonance mass. For $t\bar{t}$ production, the decay width of the color octet vector boson is relevant for $M_{V_8} > 2m_t$ so that the top pair can be produced at resonance. Earlier studies incorporated rather large values of the decay width e.g. $\Gamma_{V_8} \approx 0.1 - 0.2M_{V_8}$. We have on the other hand used the width calculated for the parameters employed in our study of the cross sections.

We explore the subspace of the parameters of the color octets which can explain the observed forward-backward asymmetry at the Tevatron as discussed in section III C and thus attempt to examine the admissibility of these data points *w.r.t.* the recently observed LHC data. As a first step, we compare the cross-section of the Tevatron and the LHC for the $t\bar{t}$ production corresponding to the same values of the couplings with a given resonant mass and the nature of the exchange current. This is shown in figure 17a where the $t\bar{t}$ cross-section induced by the flavor conserving couplings within the allowed experimental limits for Tevatron and LHC are depicted on the x and y axes respectively. To highlight the chosen data-points we mark the focus points in the figure along with prediction



$$(a) f_{LL}^{q,ut} = f_{RR}^{q,ut} = -f_{RL}^{q,ut} = -f_{LR}^{q,ut} = f_{AA}^{q,ut}$$



$$(b) f_{RR}^{q,ut} \neq 0 = f_{LR}^{q,ut} = f_{RL}^{q,ut} = f_{LL}^{q,ut}$$

FIG. 13: Variation of the combined cross-section $\sigma(p\bar{p} \rightarrow t\bar{b} + \bar{t}\bar{b})$ and $\sigma(p\bar{p} \rightarrow tj + \bar{t}\bar{j})$ with couplings $\sqrt{f_{ij}^{q,ut}}$ corresponding to different values of $M_{V_8^0}$. In the figures (a) and (b) the upper dotted black line and associated blue band depicts the central value of combined experimental $s+t$ -channel cross-section and one sigma allowed region of $3.04^{+0.57}_{-0.53}$ pb from CDF [13], while the lower dot-dashed black line with a red band show theoretical estimate and its uncertainty 3.15 ± 0.26 pb at NNNLO [4].

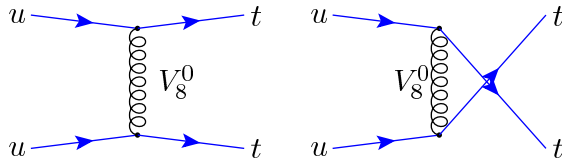


FIG. 14: Diagrams for same sign top production through V_8^0 in (a) t - and (b) u -channels.

from SM. The two vertical lines in the figure corresponds to the $1-\sigma$ boundaries of the maximum allowed $\sigma_{t\bar{t}}$ at the Tevatron [2, 3]. It is clear from the figure that the observed $\sigma_{t\bar{t}}$ at the Tevatron completely lies within the experimentally observed range of $\sigma_{t\bar{t}}$ at the LHC [51]. In Figure 17b the same is plotted for the flavor violation case.

Unlike Tevatron, LHC possess a rich potential for the new physics resonant searches both for the threshold and the boosted production of the unlike sign top pairs. The differential cross-sections for the $t\bar{t}$ production are studied in the reference [52] along with Z' and other new physics resonant searches in reference [53]. No significant deviations from the SM are observed. We investigated the one dimensional distribution of the transverse momentum of the top and the invariant mass of the top pairs. Any large deviation that might occur due to the color octet contribution in these distributions will exclude the corresponding resonant mass and the couplings. In Figure 18a and 18b we show p_T and $m_{t\bar{t}}$ distribution at the LHC for the preferred values of parameters required to obtain the experimentally observed $A_{FB}^{t\bar{t}}$. The p_T distribution as well as the $t\bar{t}$ invariant mass distribution for 7 TeV LHC data show a clear narrow resonance

for $M_{V_8} = 900$ GeV on top of the SM background. Since ATLAS and CMS [52, 53] have not yet observed any kind of such resonance effect for the p_T and $m_{t\bar{t}}$ distribution, the octet vector boson model with $M_{V_8}=900$ GeV can be excluded with the coupling constant of 0.35.

In the flavor violation case $t\bar{t}$ production proceeds through V_8^0 exchange in the t -channel and therefore no resonance effect is expected.

B. Charge Asymmetry and spin correlation

We found that the $t\bar{t}$ production data at the Tevatron shows a relatively large $A_{FB}^{t\bar{t}}$, the LHC data on the other hand exhibits a small 'charge asymmetry' A_C given by

$$A_C = \frac{N(\Delta |y| > 0) - N(\Delta |y| < 0)}{N(\Delta |y| > 0) + N(\Delta |y| < 0)}, \quad (21)$$

where $\Delta |y| = |y_t| - |y_{\bar{t}}|$ is the difference between absolute rapidities of the top and antitop quarks. In the SM both the asymmetries $A_{FB}^{t\bar{t}}$ and A_C are generated at the next to leading order (NLO) of QCD. The most recent results from the CMS [56] and the ATLAS [57] collaborations at the LHC give $A_C^{ATLAS} = -1.9 \pm 2.8(stat.) \pm 2.4(syst.)\%$ and $A_C^{CMS} = -1.3 \pm 2.8(stat.)^{+2.9}_{-3.1}(syst.)\%$. These values are consistent with the SM prediction, $A_C = 1.15 \pm 0.06\%$ within the experimental uncertainty [58].

Both the asymmetries depend on the coupling of color vector bosons with light and top quarks i.e. on the $q\bar{q} \rightarrow t\bar{t}$ process. We provide a scatter plot in figures 19a and 19b in order to study the correlation between

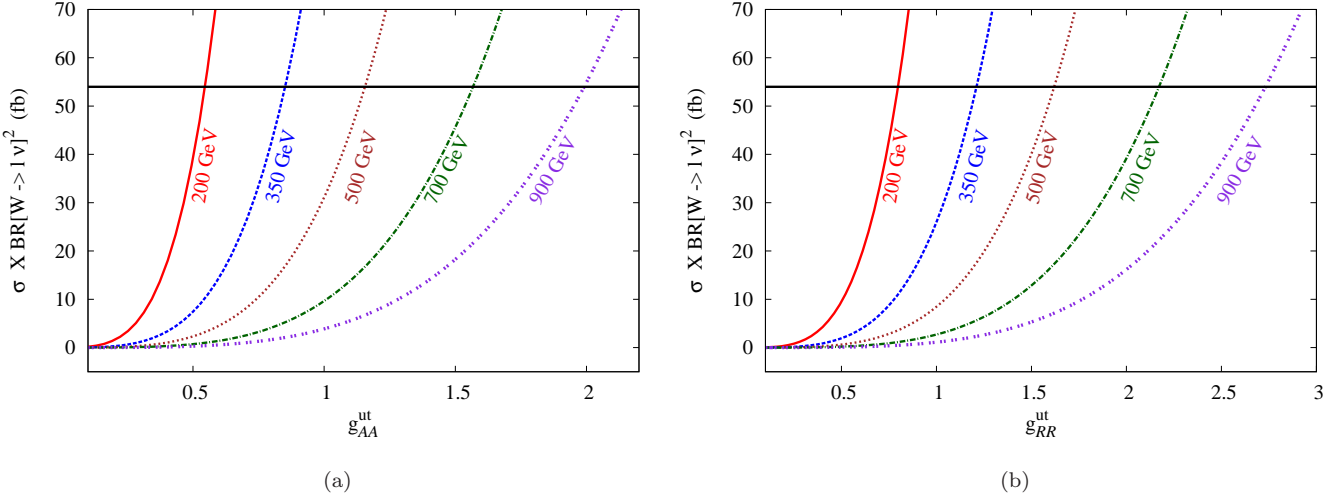


FIG. 15: Variation of the cross-section $\sigma(p\bar{p} \rightarrow tt + t\bar{t})$ times branching ratio $BR(W \rightarrow l\nu)^2$ with couplings g_{ij}^{ut} for flavor violating vector color octets corresponding to different values of $M_{V_8^0}$ GeV for both the cases (a) and (b) given in the text. The upper dotted line depicts the maximum allowed $\sigma_{tt+t\bar{t}} \times BR(W \rightarrow l\nu)^2 = 54$ fb with a 95 % confidence level [16].

$A_{FB}^{t\bar{t}}$ at the tevatron and A_C at the LHC for three different vector boson masses corresponding to FC and FV interactions. In these figures x and y coordinates depict the $A_{FB}^{t\bar{t}}$ in Tevatron and A_C at LHC respectively for a fixed value of the resonant mass and the coupling. The range of the couplings on the x axis are chosen such that it generates the appropriate $A_{FB}^{t\bar{t}}$ observed in the $t\bar{t}$ production at Tevatron. The favorable points mentioned in Tables I and III are encircled in the figure. The inner and outer pair of vertical lines corresponds to the 1- and 2- σ boundaries of the experimental forward-backward asymmetry at the Tevatron [7] while horizontal line shows the 1- σ boundary of the experimental charge asymmetry at LHC [56].

LHC provides a unique platform to study the spin and polarization distribution of top and antitop for both the threshold and boosted events. We study and compare the contribution of the color octets to the spin correlation coefficient $C^{t\bar{t}}$. To constrain the parameter space we plot the curves in the figures 20a and 20b for the flavor conserving and violating cases respectively. Each point (x, y) on the curve estimates the contribution to $C^{t\bar{t}}$ at Tevatron and LHC respectively corresponding to a fixed value of the resonant mass and the coupling. The vertical and the horizontal line depicts the experimental central values of $C^{t\bar{t}}$ at Tevatron and LHC respectively. We observe that our focus points which are highlighted in the figure are in good agreement with the experimental values within 1σ error estimations.

C. Dijet resonance searches

Recent searches for dijet resonances in 7 TeV pp collisions at ATLAS and CMS [35] provides exclusion limits

for axigluon/coloron masses. CMS data exclude axigluons and colorons with mass less than 2.47 TeV at 95 % confidence level while ATLAS exclusion limits is between 0.60 and 2.10 TeV for the same resonances.

The color octet vector bosons produced from the $q\bar{q}$ initial state will give rise to dijet events by decaying into the $q\bar{q}$ states. The dijet cross section thus depends on the same parameters namely $M_{V_8}, \Gamma_{V_8}, g_L^q$ and g_R^q as the other observables considered in the study. Whereas the $t\bar{t}$ cross section depends on the product of the couplings of the color octet vector bosons with light and top quarks $g_i^q g_j^t (i, j = L, R)$, the dijet cross section depends only on $(g_{L/R}^q)^2$ and therefore can provide a more stringent bounds on these couplings from the direct resonant searches. As discussed in the Introduction, CMS and ATLAS collaborations have performed a search of narrow dijet resonances. The dijet resonance searches are based on the narrow width approximation and therefore they do not constraint vector bosons with large width.

We study the p_T distribution of the jet with highest p_T and invariant mass distribution of the two highest p_T jets in SM and then compare the distribution with the specific choices of resonant mass along with their couplings as mentioned in Table I for flavor conserving case. It is to be noted that there is no contribution from flavor violating couplings involving the first and third generation quarks.

We have imposed the standard acceptance cuts for these distributions. The minimum dijet invariant mass m_{jj} is taken to be 200 GeV along with the required pseudorapidity separation $|\Delta\eta| \leq 1.3$ and both jets satisfying $|\eta| \leq 2.5$. We show the p_T distribution in figure 21a with the bin width 10 GeV and the invariant mass distribution of the two highest p_T jets in figure 21b with bin width 50 GeV.

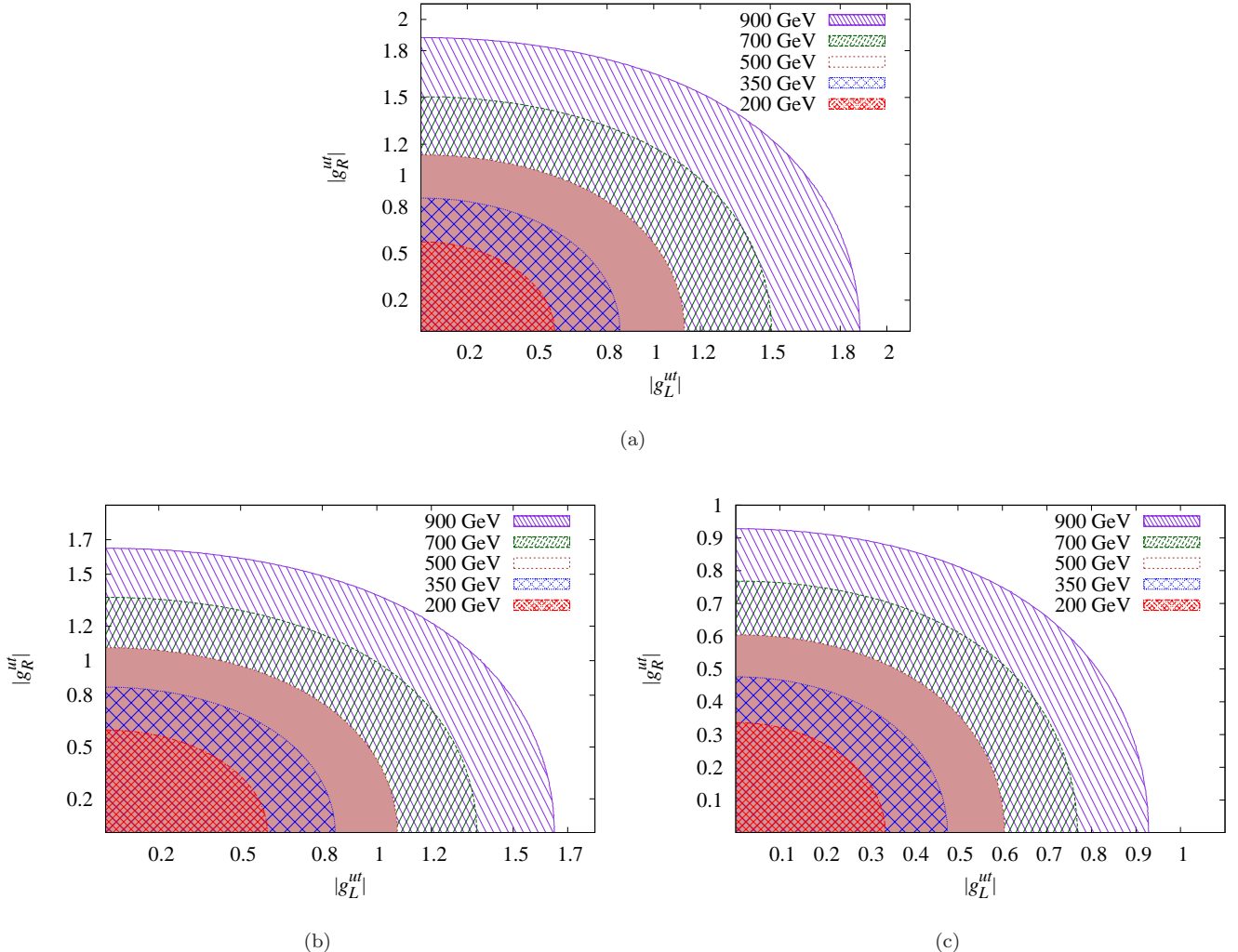


FIG. 16: 95% CL exclusion contours on the plane of g_L^{ut} and g_R^{ut} for varying color octet masses. Figure (a) corresponds to $\sigma(pp \rightarrow t\bar{t} + t\bar{t}) \times BR[W \rightarrow l\nu]^2 \leq 54 \text{ fb}$ from Tevatron at CDF [16]. Figure (b) corresponds to measurement from CMS at LHC, constraining $\sigma(pp \rightarrow tt(j)) \leq 17 \text{ pb}$ [17] and figure (c) corresponds to $\sigma(pp \rightarrow tt) \leq 1.7 \text{ pb}$ from ATLAS detector at LHC [18].

The $d\sigma/dm_{jj}$ distribution are all in good agreement with the SM QCD background within the experimental error bars except for the case of $M_{V_8} = 900 \text{ GeV}$. Therefore $M_{V_8} = 900 \text{ GeV}$ resonance can be excluded based on the resonant searches not only from the $t\bar{t}$ production but also from the dijet searches as well.

VII. SUMMARY AND CONCLUSION

We have revisited the contribution of the color octet vector boson model in the top sector at Tevatron and LHC. The observed features of the analysis for top quark physics at the Tevatron and the LHC are enumerated as follows:

1. We have studied the variation of $t\bar{t}$ cross-section in flavor conserving and flavor violating neutral cur-

rent interactions. The effect of finite decay width of the exotic colored bosons is taken into account throughout our analysis.

2. We notice appreciable contribution to $A_{FB}^{t\bar{t}}$ and spin-correlation coefficient from the axial current and the right handed chiral current without transgressing the production cross-sections within experimentally allowed one sigma region.
3. We scanned the parameter space of the model to explain the anomaly observed in one dimensional $m_{t\bar{t}}$ and $|\Delta y|$ distributions of $A_{FB}^{t\bar{t}}$. We predict few focus points based on the χ^2 minimization at χ^2_{\min} , which are likely to satisfy these constraints. This is summarized in tables I & II and in tables III & IV for the flavor conserving and flavor changing neutral currents respectively. $m_{t\bar{t}}$ distribution

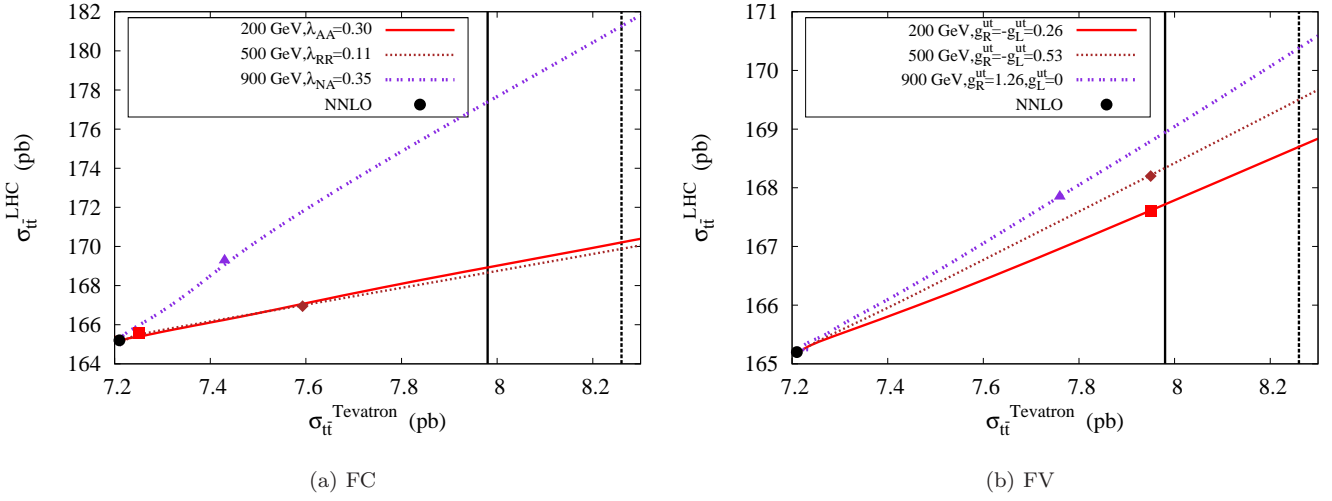


FIG. 17: The x and y coordinates on the curve depicts the production cross sections $\sigma_{t\bar{t}}$ at Tevatron and LHC respectively corresponding to a fixed value of the coupling and the resonant mass for (a) flavor conserving and (b) flavor violating cases. The highlighted colored data points corresponds to the focus points mentioned in Tables I and III. Vertical lines depicts the $1-\sigma$ boundary for CDF [2] and DØ [3] respectively as given in the text. Black point corresponds to the SM NNLO approximate value of at LHC (165.2 pb) and Tevatron (7.2 pb) [4].

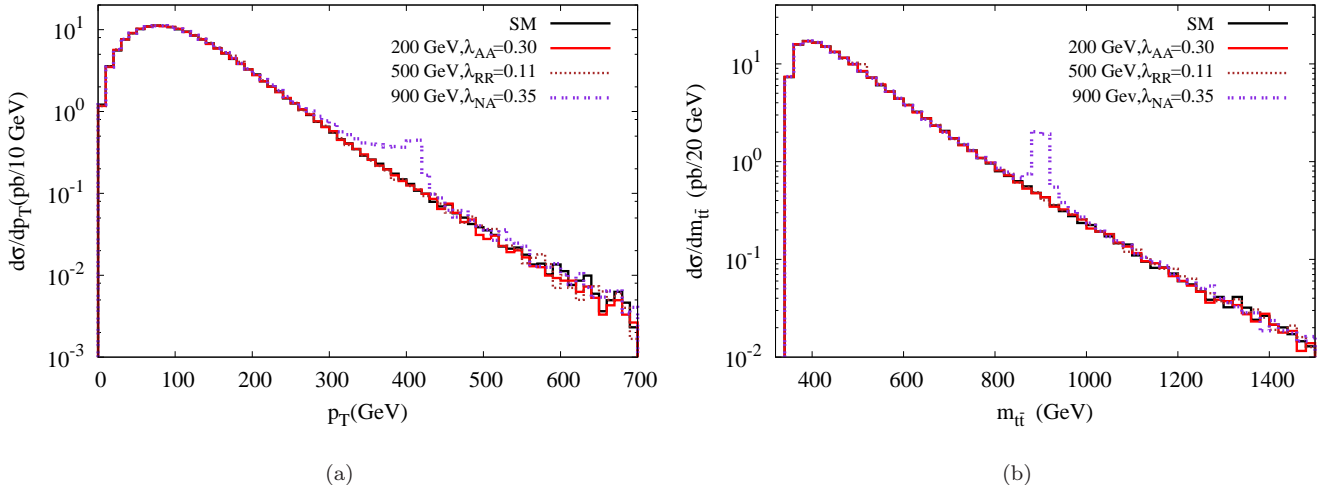


FIG. 18: The differential distribution of (a) transverse momentum of the top p_T with bin width 10 GeV and (b) top pair invariant mass with bin width 20 GeV at LHC with $\sqrt{s} = 7$ TeV corresponding to the SM and the flavor conserving focus points mentioned in Table I.

of $A_{FB}^{t\bar{t}}$ corresponding to focus points are also depicted in figures 8a, 8e, 8c and 9a, 9c, 9e for FC and FV couplings respectively. Similarly the agreement w.r.t. $|\Delta y|$ distribution is shown in figures 8b, 8f, 8d and 9b, 9d, 9f for flavor conserving and violating cases respectively.

- We verified that the top quark couplings corresponding to these focus points evade the lower bounds on the chiral couplings required to form top quark condensates [34].

5. Single top quark production through massive color charged vector boson is studied for the s and t channel separately with distinguishable final states as in SM. We observe that a large parameter region is allowed by the one and two sigma bands corresponding to s and t channels respectively from CDF [13]. Since we have performed our analysis with $|V_{tb}|^2 = 1$, we need to be careful about the interplay of new physics parameters and allowed deviation for $|V_{tb}|$ from unity.

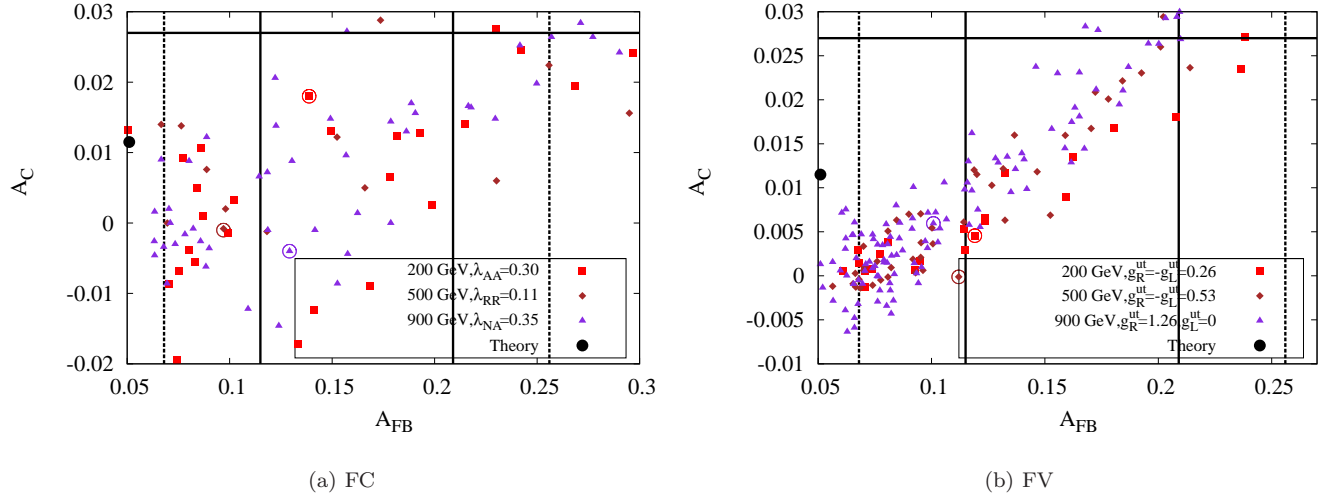


FIG. 19: The x and y coordinates of the points in the scatter plot depict the A_{FB}^{tt} at the Tevatron and A_C at the LHC respectively corresponding to a fixed value of the coupling and the resonant mass for (a) flavor conserving and (b) flavor violating cases. The encircled colored data points corresponds to the focus points mentioned in Tables I and III. The inner and outer pair of vertical lines are 1- and 2- σ boundaries of the experimental forward-backward asymmetry at the Tevatron [7] while horizontal line shows the 1- σ boundary of the experimental charge asymmetry at LHC [56].

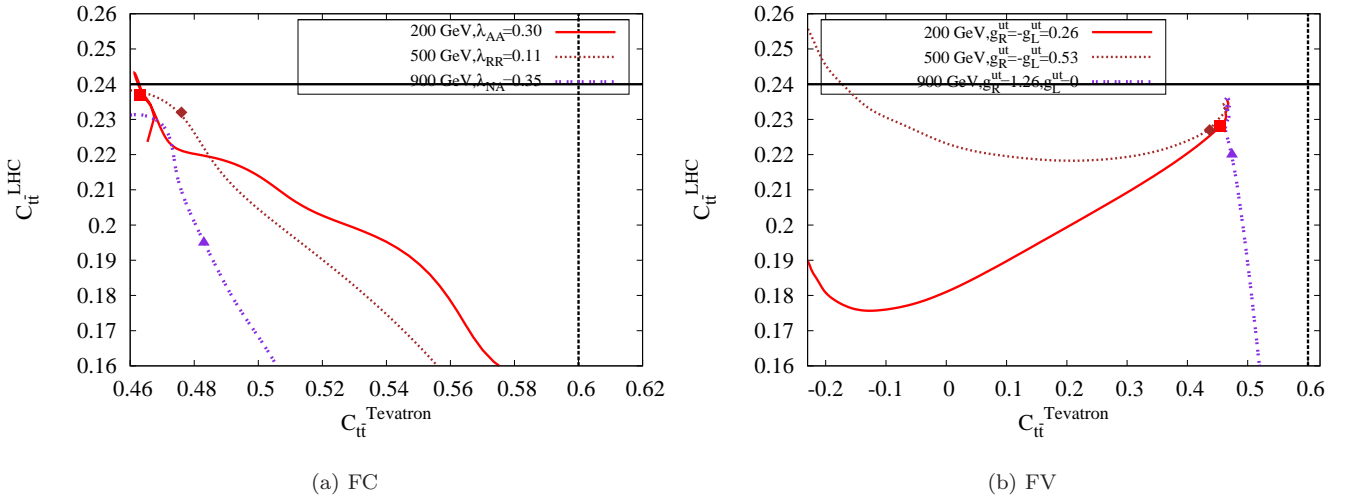


FIG. 20: The x and y coordinates on the curve depicts the spin correlation coefficients $C^{t\bar{t}}$ at Tevatron and LHC respectively corresponding to a fixed value of the coupling and the resonant mass for (a) flavor conserving and (b) flavor violating cases. The highlighted colored data points corresponds to the focus points mentioned in Tables I and III. The horizontal and vertical lines corresponds to the central values of $C^{t\bar{t}}$ in the helicity basis at the LHC [59] and the Tevatron [40] respectively.

- The introduction of flavor changing neutral current for the $t\bar{t}$ production also induces the single top production in s and t channels with the same final states. So, we compared our results with the observed combined cross-sections from s and t channels at the Tevatron. We find that the cross-section of the single top quark production is comparatively more sensitive to the new physics couplings in comparison to the $t\bar{t}$ model. We are able to constrain the product of FC and FV couplings of the neutral

current from this process.

7. Consistency of the color octet vector boson model with respect to focus points are examined in the light of recent LHC data in section VI. We probed the admissibility of the constrained parameter space at LHC which explained the required $A_{FB}^{t\bar{t}}$ at the Tevatron as mentioned in section III C. We observe that the focus points do not transgress the cross-section of the top pair production [51] as well

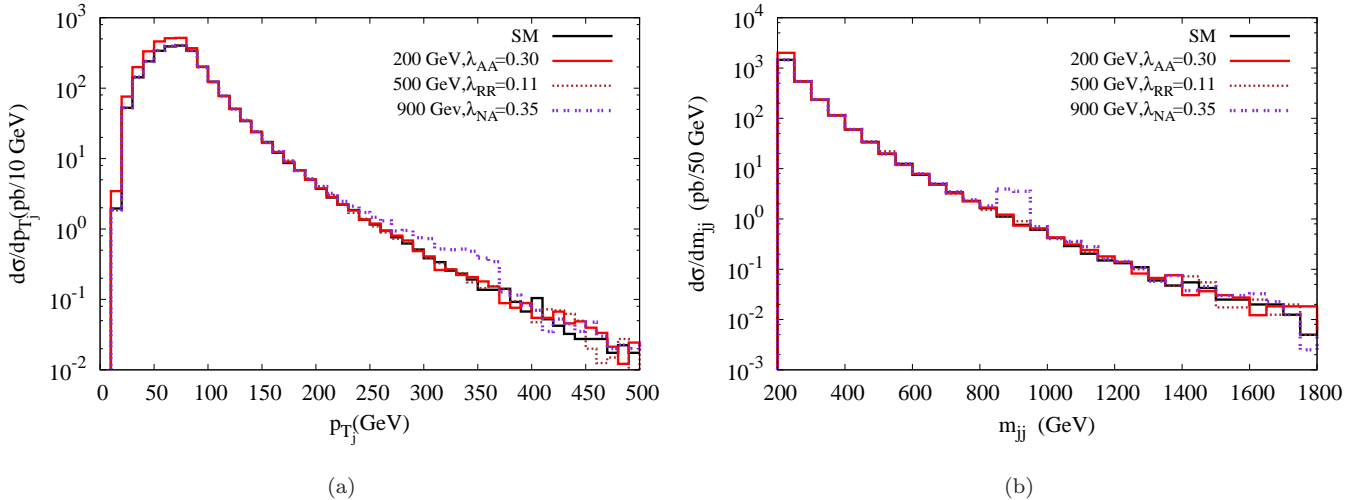


FIG. 21: The differential distribution of (a) transverse momentum of the highest p_T jet with bin width 10 GeV and (b) dijet invariant mass m_{jj} of the two highest p_T jets with bin width 50 GeV at LHC with $\sqrt{s} = 7$ TeV corresponding to the SM and the focus points mentioned in Table I for flavor conserving case.

as the measured charge asymmetry [56] and spin correlation [59] at LHC.

To have more insight on the implication of the new physics parameter space we study the p_T and $m_{t\bar{t}}$ distributions of the top pair. We find that all our FC focus points as mentioned in Table I except for the higher resonance mass of 900 GeV are consistent with the observations at LHC.

The correlation study of the $A_{FB}^{t\bar{t}}$ at Tevatron and A_C at LHC in figures 19a and 19b shows that the large $A_{FB}^{t\bar{t}}$ at Tevatron be accommodated by the recent observations at LHC within 2σ limit. The spin correlation coefficient predicted with constrained parameter space of the color excited states at LHC are also found to lie within the one σ limit of the experimental values [40, 59].

8. Since the strongest bound for the light quark couplings to the color exotics comes from the dijet searches, we studied the transverse momentum and invariant dijet mass distribution at LHC corresponding to the parameter space which generated a large $A_{FB}^{t\bar{t}}$ at Tevatron. We observe an appreciable deviation for the color octet at 900 GeV similar to that observed for $m_{t\bar{t}}$ distribution.
 9. We also studied the production cross-section of same sign top and anti top pairs *via* FV couplings at Tevatron. We imposed the constraints of non-observability of large same sign di-lepton events at Tevatron and provided the 95 % exclusion contours in the figure 16a on the plane of chiral couplings. Exclusion contours at 95 % are also computed from recent results at CMS and ATLAS for the same sign top production only which are depicted in fig-

ures 16b and 16c respectively. The constraints from LHC restrict the allowed parameter space of FV to a narrow allowed region. We observe that all focus points except one (900 GeV with $g_R^{ut} = 1.26$) corresponding to FV couplings as shown in figure 16c lies within this narrow allowed region.

Our analysis for the top quark physics in vector color octet model based on the recent observations at Tevatron and LHC has shrunk the allowed parameter space to a great extent. We propose four focus data points (two each from flavor conserving and violating couplings) which can explain the $A_{FB}^{t\bar{t}}$ anomaly at the Tevatron and are also consistent with the $t\bar{t}$, same-sign top and dijet production cross-sections and associated observables at the LHC.

Acknowledgments

The authors would like to thank Amitabha Mukherjee, Debajyoti Choudhury, Mamta Dahiya and Rashidul Islam for fruitful discussions. SD and MK likes to thank Fabio Maltoni and Rikkert Frederix for illuminating discussions on MadGraph and single top analysis. We acknowledge the partial support from DST, India under grant SR/S2/HEP-12/2006. SD and AG would like to acknowledge the UGC research award and CSIR(ES) award respectively for the partial financial support . We also thank RECAPP, HRI for local hospitality where the part of the work was done.

Appendix A: Computation of Helicity Amplitudes

1. Helicity amplitudes for $q\bar{q} \rightarrow t\bar{t}$ via flavor conserving vector octets

All couplings are in units of g_s . $g_L^q = g_L^t = g_R^q = g_R^t = 1$ for SM.

$$\begin{aligned}\mathcal{M}_{+-\pm\pm}^{V_8^0} &= \mathcal{F}_s g_R^q (g_L^t + g_R^t) \frac{\hat{s}}{2} \sqrt{1 - \beta^2} \sin \theta \\ &= \mathcal{M}_{-+\mp\mp}^{V_8} (L \leftrightarrow R, R \leftrightarrow L)\end{aligned}\quad (\text{A.1})$$

$$\begin{aligned}\mathcal{M}_{+-\pm\mp}^{V_8^0} &= \mathcal{F}_s g_R^q [(g_L^t + g_R^t) \mp \beta(g_L^t - g_R^t)] \frac{\hat{s}}{2} (1 \pm \cos \theta) \\ &= \mathcal{M}_{-+\mp\pm}^{V_8} (L \leftrightarrow R, R \leftrightarrow L)\end{aligned}\quad (\text{A.2})$$

$$\text{where, } \mathcal{F}_s = \frac{g_s^2 T^a T^a}{(\hat{s} - M_{V_8^0}^2) + i M_{V_8^0} \Gamma_{V_8^0}}$$

and T^a is the SU(3) matrices.

2. Helicity amplitudes for $q\bar{q} \rightarrow t\bar{t}$ via flavor violating vector octets

$$\begin{aligned}\mathcal{M}_{++\pm\pm}^{V_8} &= \mathcal{F}_t g_R^{ut} g_L^{ut} \hat{s} (1 \pm \beta) \\ &= \mathcal{M}_{-\mp\mp}^{V_8} (L \leftrightarrow R, R \leftrightarrow L)\end{aligned}\quad (\text{A.3})$$

$$\begin{aligned}\mathcal{M}_{+-\pm\pm}^{V_8} &= \mathcal{F}_t g_R^{ut} \frac{\hat{s}}{2} \sqrt{1 - \beta^2} \sin \theta \\ &= \mathcal{M}_{-+\pm\pm}^{V_8} (L \leftrightarrow R, R \leftrightarrow L)\end{aligned}\quad (\text{A.4})$$

$$\begin{aligned}\mathcal{M}_{+-\pm\mp}^{V_8} &= \mathcal{F}_t g_R^{ut} \frac{\hat{s}}{2} (1 \pm \beta) (1 \pm \cos \theta) \\ &= \mathcal{M}_{-+\mp\pm}^{V_8} (L \leftrightarrow R, R \leftrightarrow L)\end{aligned}\quad (\text{A.5})$$

$$\text{where, } \mathcal{F}_t = \frac{g_s^2 T^a T^a}{(\hat{t} - M_{V_8^0}^2) + i M_{V_8^0} \Gamma_{V_8^0}}$$

-
- [1] T. T. E. W. Group [CDF and D0 Collaboration], arXiv:1007.3178 [hep-ex].
[2] CDF Note 9913.
[3] V. M. Abazov *et al.* [D0 Collaboration], Phys. Lett. B **704**, 403 (2011) [arXiv:1105.5384 [hep-ex]].
[4] N. Kidonakis, arXiv:1205.3453 [hep-ph]; N. Kidonakis, Phys. Rev. D **82**, 114030 (2010) [arXiv:1009.4935 [hep-ph]]; N. Kidonakis, arXiv: 1105.3481 [hep-ph]; N. Kidonakis, arXiv:0909.0037 [hep-ph].
[5] T. Aaltonen *et al.* [CDF Collaboration], Phys. Rev. D **83**, 112003 (2011) [arXiv:1101.0034 [hep-ex]]; CDF Note 10436; CDF Note 10584.
[6] V. M. Abazov *et al.* [D0 Collaboration], Phys. Rev. D **84**, 112005 (2011) [arXiv:1107.4995 [hep-ex]].
[7] CDF Note 10807, 2012.
[8] S. Frixione, P. Nason, and G. Ridolfi, JHEP 0709 (2007) 126; N. Kidonakis, Phys. Rev. D **84**, 011504 (2011); V. Ahrens, A. Ferroglio, M. Neubert, B. D. Pecjak, and L.L. Yang, Phys. Rev. D **84**, 074004 (2011); W. Hollik and D. Pagani, Phys. Rev. D **84**, 093003 (2011); J. Kühn and G. Rodrigo, JHEP 1201 (2012) 063 [arXiv:1109.6830]; A. V. Manohar and M. Trott, arXiv:1201.3926 [hep-ph].
[9] M. Dahiya, S. Dutta and R. Islam, arXiv:1206.5447 [hep-ph].
[10] J. Shu, K. Wang and G. Zhu, Phys. Rev. D **85**, 034008 (2012) [arXiv:1104.0083 [hep-ph]]; M. I. Gresham, I. -W. Kim and K. M. Zurek, Phys. Rev. D **83**, 114027 (2011) [arXiv:1103.3501 [hep-ph]]; D. Duffy, Z. Sullivan, and H. Zhang, arXiv:1203.4489. M. I. Gresham, I. -W. Kim and K. M. Zurek, Phys. Rev. D **83**, 114027 (2011) [arXiv:1103.3501 [hep-ph]].
[11] J. A. Aguilar-Saavedra and M. Perez-Victoria, JHEP **1109**, 097 (2011) [arXiv:1107.0841 [hep-ph]]; J. A. Aguilar-Saavedra and M. Perez-Victoria, Phys. Rev. D **84**, 115013 (2011) [arXiv:1105.4606 [hep-ph]].
[12] See, e.g., the following and references therein: Q. -H. Cao, D. McKeen, J. L. Rosner, G. Shaughnessy and C. E. M. Wagner, Phys. Rev. D **81**, 114004 (2010).
[13] CDF Note 10793.
[14] V. M. Abazov *et al.* [D0 Collaboration], Phys. Rev. D **84**, 112001 (2011) [arXiv:1108.3091 [hep-ex]].
[15] CMS Collaboration: CMS-PAS-TOP-10-008.
[16] CDF report 10466.
[17] S. Chatrchyan *et al.* [CMS Collaboration], JHEP **1108**, 005 (2011) [arXiv:1106.2142 [hep-ex]].
[18] G. Aad *et al.* [ATLAS Collaboration], JHEP **1204**, 069 (2012) [arXiv:1202.5520 [hep-ex]].
[19] S. Jung, H. Murayama, A. Pierce and J. D. Wells, Phys. Rev. D **81**, 015004 (2010) [arXiv:0907.4112 [hep-ph]].
[20] K. Cheung, W. -Y. Keung and T. -C. Yuan, Phys. Lett. B **682**, 287 (2009) [arXiv:0908.2589 [hep-ph]].
[21] K. Agashe, A. Belyaev, T. Krupovnickas, G. Perez and J. Virzi, Phys. Rev. D **77**, 015003 (2008) [arXiv:hep-ph/0612015]; B. Lillie, L. Randall and L. T. Wang, JHEP **0709**, 074 (2007) [arXiv:hep-ph/0701166]; B. Lillie, J. Shu and T. M. P. Tait, Phys. Rev. D **76**, 115016 (2007) [arXiv:0706.3960 [hep-ph]].
[22] For SUSY R-parity violating interactions, see a review, R. Barbier *et al.*, Phys. Rept. **420**, 1 (2005) [arXiv:hep-ph/0406039], and references therein.
[23] N. Cabibbo, L. Maiani and Y. Srivastava, Phys. Lett. B **139**, 459 (1984); A. De Rujula, L. Maiani and R. Petronzio, Phys. Lett. B **140**, 253 (1984); J. H. Kuhn and P. M. Zerwas, Phys. Lett. B **147**, 189 (1984).
[24] U. Baur, I. Hinchliffe and D. Zeppenfeld, Int. J. Mod. Phys. A **2**, 1285 (1987); U. Baur, M. Spira and P. M. Zerwas, Phys. Rev. D **42**, 815 (1990).
[25] J. L. Hewett and T. G. Rizzo, Phys. Rept. **183**, 193 (1989).
[26] B. A. Dobrescu, K. Kong and R. Mahbubani, JHEP **0707**, 006 (2007) [arXiv:hep-ph/0703231]; B. A. Dobrescu, K. Kong and R. Mahbubani, Phys. Lett. B **670**, 119 (2008) [arXiv:0709.2378 [hep-ph]].
[27] J. Shu, T. M. P. Tait and K. Wang, Phys. Rev. D **81**, 034012 (2010) [arXiv:0911.3237 [hep-ph]]; A. Arhrib, R. Benbrik and C. -H. Chen, Phys. Rev. D **82**, 034034 (2010) [arXiv:0911.4875 [hep-ph]]; Z. Ligeti, G. M. Tavares and M. Schmaltz, JHEP **1106** (2011) 109 [arXiv:1103.2757 [hep-ph]]; I. Dorsner, S. Fajfer,

- J. F. Kamenik and N. Kosnik, Phys. Rev. D **81**, 055009 (2010) [arXiv:0912.0972 [hep-ph]]; J. C. Pati and A. Salam, Phys. Rev. D **10**, 275 (1974) [Erratum-ibid. D **11**, 703 (1975)]; R. N. Mohapatra and R. E. Marshak, Phys. Rev. Lett. **44**, 1316 (1980) [Erratum-ibid. **44**, 1643 (1980)]; Z. Chacko and R. N. Mohapatra, Phys. Rev. D **59**, 055004 (1999) [arXiv:hep-ph/9802388].
- [28] S. Cullen, M. Perelstein and M. E. Peskin, Phys. Rev. D **62**, 055012 (2000) [arXiv:hep-ph/0001166]; P. Burikham, T. Figy and T. Han, Phys. Rev. D **71**, 016005 (2005) [Erratum-ibid. D **71**, 019905 (2005)] [arXiv:hep-ph/0411094]; Z. Dong, T. Han, M. X. Huang and G. Shiu, JHEP **1009**, 048 (2010) [arXiv:1004.5441 [hep-ph]]; L. A. Anchordoqui, H. Goldberg and T. R. Taylor, Phys. Lett. B **668**, 373 (2008) [arXiv:0806.3420 [hep-ph]]; L. A. Anchordoqui, H. Goldberg, D. Lust, S. Nawata, S. Stieberger and T. R. Taylor, Phys. Rev. Lett. **101**, 241803 (2008) [arXiv:0808.0497 [hep-ph]].
- [29] C. T. Hill and E. H. Simmons, Phys. Rept. **381**, 235 (2003) [Erratum-ibid. **390**, 553 (2004)] [arXiv:hep-ph/0203079], and references therein.
- [30] G. Z. Krnjaic, Phys. Rev. D **85**, 014030 (2012) [arXiv:1109.0648 [hep-ph]]; D. Choudhury, R. M. Godbole, S. D. Rindani and P. Saha, Phys. Rev. D **84**, 014023 (2011) [arXiv:1012.4750 [hep-ph]]; P. Ferrario and G. Rodrigo, Phys. Rev. D **80**, 051701 (2009) [arXiv:0906.5541 [hep-ph]]; P. H. Frampton, J. Shu and K. Wang, Phys. Lett. B **683**, 294 (2010) [arXiv:0911.2955 [hep-ph]]; P. H. Frampton and S. L. Glashow, Phys. Lett. B **190**, 157 (1987); J. Bagger, C. Schmidt and S. King, Phys. Rev. D **37**, 1188 (1988); J. A. Aguilar-Saavedra and M. Perez-Victoria, Phys. Lett. B **705**, 228 (2011) [arXiv:1107.2120 [hep-ph]]; A. R. Zerwekh, Eur. Phys. J. C **65**, 543 (2010) [arXiv:0908.3116 [hep-ph]]; A. R. Zerwekh, Phys. Lett. B **704**, 62 (2011) [arXiv:1103.0956 [hep-ph]]; R. S. Chivukula, E. H. Simmons and C. -P. Yuan, Phys. Rev. D **82**, 094009 (2010) [arXiv:1007.0260 [hep-ph]]; G. Marques Tavares and M. Schmaltz, Phys. Rev. D **84**, 054008 (2011) [arXiv:1107.0978 [hep-ph]].
- [31] H. Wang, Y. -k. Wang, B. Xiao and S. -h. Zhu, Phys. Rev. D **84**, 094019 (2011) [arXiv:1107.5769 [hep-ph]].
- [32] X. -P. Wang, Y. -K. Wang, B. Xiao, J. Xu and S. -h. Zhu, Phys. Rev. D **83**, 115010 (2011) [arXiv:1104.1917 [hep-ph]].
- [33] J. Sayre, D. A. Dicus, C. Kao and S. Nandi, Phys. Rev. D **84**, 015011 (2011) [arXiv:1105.3219 [hep-ph]]; D. A. Dicus, C. Kao, S. Nandi and J. Sayre, Phys. Rev. D **83**, 091702 (2011) [arXiv:1012.5694 [hep-ph]]; I. Bertram and E. H. Simmons, Phys. Lett. B **443**, 347 (1998) [hep-ph/9809472]; E. H. Simmons, Phys. Rev. D **55**, 1678 (1997) [hep-ph/9608269]; A. Atre, R. S. Chivukula, P. Ittisamai, E. H. Simmons and J. -H. Yu, arXiv:1206.1661 [hep-ph]; H. X. Zhu, C. S. Li, D. Y. Shao, J. Wang and C. P. Yuan, arXiv:1201.0672 [hep-ph]; R. S. Chivukula, A. Farzinnia, E. H. Simmons and R. Foadi, Phys. Rev. D **85**, 054005 (2012) [arXiv:1111.7261 [hep-ph]]; L. M. Carpenter and S. Mantry, Phys. Lett. B **703**, 479 (2011) [arXiv:1104.5528 [hep-ph]]; B. Xiao, Y. -k. Wang and S. -h. Zhu, arXiv:1011.0152 [hep-ph]; A. R. Zerwekh, Eur. Phys. J. C **70**, 917 (2010) [arXiv:1008.4575 [hep-ph]].
- [34] C. T. Hill, Phys. Lett. B **266**, 419 (1991); C. T. Hill and S. J. Parke, Phys. Rev. D **49**, 4454 (1994) [arXiv:hep-ph/9312324]; R. S. Chivukula, A. G. Cohen and E. H. Simmons, Phys. Lett. B **380**, 92 (1996) [arXiv:hep-ph/9603311].
- [35] S. Chatrchyan *et al.* [CMS Collaboration], Phys. Lett. B **704**, 123 (2011) [arXiv:1107.4771 [hep-ex]]; G. Aad *et al.* [ATLAS Collaboration], Phys. Rev. Lett. **105**, 161801 (2010) [arXiv:1008.2461 [hep-ex]].
- [36] T. Han, I. Lewis and Z. Liu, JHEP **1012**, 085 (2010) [arXiv:1010.4309 [hep-ph]].
- [37] J. Alwall, P. Demin, S. de Visscher, R. Frederix, M. Herquet, F. Maltoni, T. Plehn and D. L. Rainwater *et al.*, JHEP **0709**, 028 (2007) [arXiv:0706.2334 [hep-ph]].
- [38] Oscar Antunano, Johann H. Kuhn, German Rodrigo, Phys. Rev. D **77**, 014003 (2008) [arXiv:0709.1652 [hep-ph]]; M.T. Bowen, S.D. Ellis, D. Rainwater, Phys. Rev. D **73**, 014008 (2006) [arXiv:hep-ph/0509267]; S. Dittmaier, P. Uwer, S. Weinzierl, Phys. Rev. Lett. **98**, 262002 (2007) [arXiv:hep-ph/0703120].
- [39] W. Bernreuther and Z. -G. Si, Nucl. Phys. B **837**, 90 (2010) [arXiv:1003.3926 [hep-ph]].
- [40] T. Aaltonen *et al.* [CDF Collaboration], Phys. Rev. D **83**, 031104 (2011) [arXiv:1012.3093 [hep-ex]].
- [41] CDF note 10719-CONF [http://www-cdf.fnal.gov/physics/new/top/2011/] V. M. Abazov *et al.* [D0 Collaboration], Phys. Lett. B **702**, 16 (2011) [arXiv:1103.1871 [hep-ex]].
- [42] P. Ko, Y. Omura and C. Yu, Nuovo Cim. C **035N3**, 245 (2012) [arXiv:1201.1352 [hep-ph]]; D. -W. Jung, P. Ko, J. S. Lee and S. -h. Nam, Phys. Lett. B **691**, 238 (2010) [arXiv:0912.1105 [hep-ph]]; D. -W. Jung, P. Ko and J. S. Lee, Phys. Lett. B **701**, 248 (2011) [arXiv:1011.5976 [hep-ph]]; D. -W. Jung, P. Ko and J. S. Lee, Phys. Lett. B **708**, 157 (2012) [arXiv:1111.3180 [hep-ph]]; D. -W. Jung, P. Ko and J. S. Lee, Phys. Rev. D **84**, 055027 (2011) [arXiv:1104.4443 [hep-ph]]; P. Ko, Y. Omura and C. Yu, Phys. Rev. D **85**, 115010 (2012) [arXiv:1108.0350 [hep-ph]]; P. Ko, Y. Omura and C. Yu, JHEP **1201**, 147 (2012) [arXiv:1108.4005 [hep-ph]]; P. Ko, Y. Omura and C. Yu, arXiv:1205.0407 [hep-ph].
- [43] C. Kao, Phys. Lett. B **348**, 155 (1995) [hep-ph/9411337]; C. -S. Li, R. J. Oakes, J. M. Yang and C. P. Yuan, Phys. Lett. B **398**, 298 (1997) [hep-ph/9701350]; S. Gopalakrishna, T. Han, I. Lewis, Z. -g. Si and Y. -F. Zhou, Phys. Rev. D **82**, 115020 (2010) [arXiv:1008.3508 [hep-ph]]; R. M. Godbole, K. Rao, S. D. Rindani and R. K. Singh, JHEP **1011**, 144 (2010) [arXiv:1010.1458 [hep-ph]]; C. Kao and D. Wackerth, Phys. Rev. D **61**, 055009 (2000) [hep-ph/9902202]; K. -i. Hikasa, J. M. Yang and B. -L. Young, Phys. Rev. D **60**, 114041 (1999) [hep-ph/9908231]; P. -Y. Li, G. -R. Lu, J. M. Yang and H. Zhang, Eur. Phys. J. C **51**, 163 (2007) [hep-ph/0608223]; J. Cao, L. Wu and J. M. Yang, Phys. Rev. D **83**, 034024 (2011) [arXiv:1011.5564 [hep-ph]].
- [44] D. Chang, S. -C. Lee and A. Soumarakov, Phys. Rev. Lett. **77**, 1218 (1996) [hep-ph/9512417]; S. Fajfer, J. F. Kamenik and B. Melic, arXiv:1205.0264 [hep-ph].
- [45] G. L. Kane, G. A. Ladinsky and C. P. Yuan, Phys. Rev. D **45**, 124 (1992).
- [46] M. Arai, N. Okada, K. Smolek and V. Simak, Phys. Rev. D **75**, 095008 (2007) [hep-ph/0701155].
- [47] J. M. Campbell, R. Frederix, F. Maltoni and F. Tramontano, Phys. Rev. Lett. **102**, 182003 (2009) [arXiv:0903.0005 [hep-ph]].
- [48] J. M. Campbell, R. Frederix, F. Maltoni and F. Tramontano, Phys. Rev. Lett. **102**, 182003 (2009) [arXiv:0903.0005 [hep-ph]].

- tano, JHEP **0910**, 042 (2009) [arXiv:0907.3933 [hep-ph]].
- [49] F. Maltoni, G. Ridolfi and M. Ubiali, arXiv:1203.6393 [hep-ph].
- [50] U. Haisch and S. Westhoff, JHEP **1108**, 088 (2011) [arXiv:1106.0529 [hep-ph]].
- [51] ATLAS-CONF-2012-134
- [52] S. Chatrchyan *et al.* [CMS Collaboration], arXiv:1211.2220 [hep-ex]; S. Chatrchyan *et al.* [CMS Collaboration], [arXiv:1209.4397 [hep-ex]].
- [53] S. Chatrchyan *et al.* [CMS Collaboration], arXiv:1211.3338 [hep-ex]; G. Aad *et al.* [ATLAS Collaboration], arXiv:1211.2202 [hep-ex];
- [54] G. Aad *et al.* [ATLAS Collaboration], JHEP **1209**, 041 (2012) [arXiv:1207.2409 [hep-ex]]; G. Aad *et al.* [ATLAS Collaboration], Eur. Phys. J. C **72**, 2083 (2012) [arXiv:1205.5371 [hep-ex]].
- [56] S. Chatrchyan *et al.* [CMS Collaboration], Phys. Lett. B **709**, 28 (2012) [arXiv:1112.5100 [hep-ex]].
- [57] G. Aad *et al.* [ATLAS Collaboration], Eur. Phys. J. C **72**, 2039 (2012) [arXiv:1203.4211 [hep-ex]].
- [58] J. H. Kuhn and G. Rodrigo, JHEP **1201**, 063 (2012) [arXiv:1109.6830 [hep-ph]].
- [59] CMS PAS TOP-12-004; G. Aad *et al.* [ATLAS Collaboration], Phys. Rev. Lett. **108**, 212001 (2012) [arXiv:1203.4081 [hep-ex]].